# NAVAL POSTGRADUATE SCHOOL
# MONTEREY, CALIFORNIA

## THESIS

## FACTORS AFFECTING THE IMPACT TOUGHNESS OF ULTRA LOW CARBON STEEL WELD METAL

by

Mary Elizabeth Gwin

September 1996

Thesis Advisor: Alan G. Fox

Thesis
G965

**Approved for public release; distribution is unlimited.**

DUDLEY KNOX LIBRARY
NAVAL POSTGRADUATE SCHOOL
MONTEREY CA 93943-5101

| | |
|---|---|
| REPORT DOCUMENTATION PAGE | Form Approved OMB No. 0704-0188 |

Public reporting burden for this collection of information is estimated to average 1 hour per response, including the time for reviewing instruction, searching existing data sources, gathering and maintaining the data needed, and completing and reviewing the collection of information. Send comments regarding this burden estimate or any other aspect of this collection of information, including suggestions for reducing this burden, to Washington Headquarters Services, Directorate for Information Operations and Reports, 1215 Jefferson Davis Highway, Suite 1204, Arlington, VA 22202-4302, and to the Office of Management and Budget, Paperwork Reduction Project (0704-0188) Washington DC 20503.

| | | |
|---|---|---|
| 1. AGENCY USE ONLY *(Leave blank)* | 2. REPORT DATE<br>September 1996 | 3. REPORT TYPE AND DATES COVERED<br>Master's Thesis |

| | |
|---|---|
| 4. TITLE AND SUBTITLE<br>FACTORS AFFECTING THE IMPACT TOUGHNESS OF ULTRA LOW CARBON STEEL WELD METAL | 5. FUNDING NUMBERS |
| 6. AUTHOR(S) Gwin, Mary E. | |
| 7. PERFORMING ORGANIZATION NAME(S) AND ADDRESS(ES)<br>Naval Postgraduate School<br>Monterey CA 93943-5000 | 8. PERFORMING ORGANIZATION REPORT NUMBER |
| 9. SPONSORING/MONITORING AGENCY NAME(S) AND ADDRESS(ES)<br>Naval Surface Warfare Center, Carderock Division, 9500 McArthur Boulevard ,Bethesda, Maryland 20084-5000 | 10. SPONSORING/MONITORING AGENCY REPORT NUMBER |

11. SUPPLEMENTARY NOTES The views expressed in this thesis are those of the author and do not reflect the official policy or position of the Department of Defense or the U.S. Government.

| | |
|---|---|
| 12a. DISTRIBUTION/AVAILABILITY STATEMENT<br>Approved for public release; distribution is unlimited. | 12b. DISTRIBUTION CODE |

13. ABSTRACT *(maximum 200 words)*

The fundamental factors affecting the impact toughness of four gas metal arc welds (GMAW) made on HSLA-100 base plate using a newly developed steel weld wire were studied. The weld metal analysis included chemistry, mechanical testing (hardness, CVN/FATT), as well as optical, scanning and transmission electron microscopy. Studies of inclusion composition using energy dispersive x-ray (EDX), and electron energy loss spectroscopy (EELS) in the transmission electron microscope were also performed.

It was found that increasing oxygen content of the weld metal (due to increased oxygen in the shielding gas) led to increased non-metallic inclusion size and volume fraction; which in turn, led to both decreasing strength and toughness. The strength was lowered because increasing oxygen in the shielding gas led to increased 'consumption' of strengthening alloys such as carbon, manganese and silicon. The toughness was compromised by the increasing size and number of oxide inclusions as these provide sites for void formation and subsequent fracture.

| | |
|---|---|
| 14. SUBJECT TERMS HSLA-100, Gas Metal Arc Welding, Ultra Low Carbon Steel, Non-Metallic Inclusions | 15. NUMBER OF PAGES 102 |
| | 16. PRICE CODE |

| | | | |
|---|---|---|---|
| 17. SECURITY CLASSIFICATION OF REPORT<br>Unclassified | 18. SECURITY CLASSIFICATION OF THIS PAGE<br>Unclassified | 19. SECURITY CLASSIFICATION OF ABSTRACT<br>Unclassified | 20. LIMITATION OF ABSTRACT<br>UL |

**Approved for public release; distribution is unlimited.**

# FACTORS AFFECTING THE IMPACT TOUGHNESS OF ULTRA LOW CARBON STEEL WELD METAL

Mary E. Gwin
Lieutenant Commander, United States Navy
B.S., United States Naval Academy, 1984

Submitted in partial fulfillment
of the requirements for the degree of

**MASTER OF SCIENCE IN MECHANICAL ENGINEERING**

from the

**NAVAL POSTGRADUATE SCHOOL**
**September 1996**

Thesis
G965
c.2

DUDLEY KNOX LIBRARY
NAVAL POSTGRADUATE SCHOO
MONTEREY CA 93943-5101

# ABSTRACT

The fundamental factors affecting the impact toughness of four gas metal arc welds (GMAW) made on HSLA-100 base plate using a newly developed steel weld wire were studied. The weld metal analysis included chemistry, mechanical testing (hardness, CVN/FATT), as well as optical, scanning and transmission electron microscopy. Studies of inclusion composition using energy dispersive x-ray (EDX), and electron energy loss spectroscopy (EELS) in the transmission electron microscope were also performed.

It was found that increasing oxygen content of the weld metal (due to increased oxygen in the shielding gas) led to increased non-metallic inclusion size and volume fraction; which in turn, led to both decreasing strength and toughness. The strength was lowered because increasing oxygen in the shielding gas led to increased 'consumption' of strengthening alloys such as carbon, manganese and silicon. The toughness was compromised by the increasing size and number of oxide inclusions as these provide sites for void formation and subsequent fracture.

## TABLE OF CONTENTS

I. INTRODUCTION ..... 1

II. BACKGROUND ..... 3

  A. HIGH STRENGTH STEEL ..... 3

    1. HY-100 ..... 3

    2. HSLA-100 ..... 4

  B. GAS METAL ARC WELDING (GMAW ..... 5

  C. ULTRA LOW CARBON FILLER WIRE ..... 6

  D. WELD METAL MICROSTRUCTURE ..... 7

    1. Non-Metallic Inclusions ..... 9

    2. Characterization of Inclusions in High Strength Steel Weld Metal ..... 9

    3. Transformation Kinetics ..... 12

  E. MECHANICAL PROPERTIES ..... 13

III. EXPERIMENTAL PROCEDURE ..... 25

  A. WELD SAMPLES ..... 25

  B. SAMPLE PREPARATION ..... 25

  C. SCANNING ELECTRON MICROSCOPY ..... 25

  D. TRANSMISSION ELECTRON MICROSCOPY ..... 26

  E. OPTICAL MICROSCOPY ..... 27

  F. MICROHARDNESS MEASUREMENTS ..... 28

  G. MECHANICAL TESTING ..... 28

  H. ERROR ..... 29

IV. ANALYSIS, RESULTS, AND DISCUSSION ..... 53

  A. WELD METAL CHEMISTRY ..... 53

  B. N0N-METALLIC INCLUSIONS ..... 55

    1. Size and Volume Fraction ..... 55

    2. Inclusion Chemical Composition ..... 55

C. MECHANICAL PROPERTIES ....................57
1. Yield Strength.... ....................57
2. Impact Properties... ....................57
D. FRACTOGRAPHY....................58
E. MICROSTRUCTURAL AND MACROSTRUCTURAL ANAYSIS..... ....................58
1. Macroscopic....................58
2. Microscopic.. ....................59
V. SUMMARY.. ....................61
A. CONCLUSIONS....................61
B. RECOMMENDATIONS....................61
LIST OF REFERENCES..... ....................87
INITIAL DISTRIBUTION LIST....................91

# ACKNOWLEDGMENTS

I owe my deepest thanks to my parents, Hal and Joy, and my brother and sister in law, Sanders and Doreen, for their love and support, and interest in all things scientific.

Special acknowledgment is due to Richard Hashimoto and Dr. Sarath Menon for assistance in the laboratory.

Finally, I owe deep appreciation to Dr. Alan Fox for his enthusiasm, humor, and guidance during the course of this thesis.

# I. INTRODUCTION

HY-100 is the primary high strength steel used in US Navy shipbuilding today. While HY-100 is the workhorse of modern shipbuilding, this steel requires highly trained welders and careful temperature control (preheat/interpass) of weld metal cooling to prevent cracking. In order to reduce in process fabrication control, and the resulting shipbuilding and repair costs, the US Navy has undertaken a research program to develop a new welding consumable for high yield strength steels (above 100 ksi). The goal of this research program is:

- to develop a welding consumable which can be deposited over a wide range of heat inputs and cooling rates without the need for interpass and preheat temperature control, and
- to fundamentally understand the metallurgical reasons behind the success of the developed wire.[Ref.1]

In order to meet these research goals, the Naval Surface Warfare Center (NSWC), Carderock Division, Bethesda, Md., in conjunction with, the Naval Postgraduate School, has undertaken the task of developing a solid filler wire for use in the Gas Metal Arc Welding (GMAW) of High Strength Low Alloy (HSLA-100) steel.[Ref.1] Once developed, the filler wire must meet the mechanical property requirements of MIL-120S as outlined in the Military Specification for Electrodes and Rods - Welding, Bare, Solid, or Alloyed Cored, Low Alloy Steel (MIL-E-23765/2E(SH). MIL-120S requires the following mechanical properties for the as-welded GMAW welds:

- Yield strength between 703 MPa (102 ksi) and 848 MPa (123 ksi), and
- Charpy V-notch minimum toughness of 61 J (45 ft-lb.) at -51$^0$ C (-60° F), and 81 J (60 ft-lb.) at -18$^0$ C (0° F).[Ref.2]

The purpose of the present study is to investigate the fundamental characteristics of gas metal arc welds consisting of HSLA-100 as the base plate material, and an experimental ultra low carbon steel filler wire (solid). Four GMAW welds were produced by NSWC with varying cover gas combinations in order to analyze the effect of weld metal oxygen content on non-metallic inclusion size / chemistry, microstructure, and resulting mechanical properties.

# II. BACKGROUND

## A. HIGH STRENGTH STEELS

HY-100 steels, which are extensively used in the shipbuilding industry, require strict control of heat input, cooling rate, and welding procedures, in order to prevent hydrogen induced cracking in the heat affected zone of welds. This high level of in-process, and post-production, fabrication control results in increased costs for shipbuilding and repair. HSLA-100 steels were developed in order to provide similar strength characteristics as HY-100 steels without the limitations and costs necessary to prevent cracking. The improved weldability of HSLA-100 has been achieved by reducing the carbon content from around 0.15 wt. % (HY-100) to about 0.06 wt. % (HSLA) and offsetting the strength losses due to reduced carbon content by increasing the alternative alloy content (copper and nickel). This is graphically illustrated in Figure 2-1. Table 2-1 illustrates the major elements which compose HY-100, HSLA-100, and the filler wire used in this study.

### 1. HY-100 Steel

The addition of alloys to iron provides a method to improve the properties of the pure metal. The main purpose of alloying in high strength steels is to increase the strength of the material while maintaining favorable impact and toughness properties. While HY-100 and HSLA-100 have similar strength and toughness, the method of achieving these properties is entirely different.

HY-100 is essentially a martensitic steel containing 0.13-0.17 wt.% carbon that has been tempered to achieve specified strength and toughness. Martensite is the hardest, strongest, and least ductile microstructure that may be formed for a given steel. The ability of a steel to form martensite is termed hardenability and is most strongly affected by the alloy addition of carbon. Carbon, as a solid solution strengthener and an interstitial impurity, acts as an impediment to dislocation motion and reduces the steels ductility. The higher the percentage of carbon in a given steel, the higher the hardenability[Ref.3].

Tempering martensitic steel, allows a very hard and strong microstructure some measure of ductility. Tempering refers to the practice of raising the temperature of a martensitic steel to allow for the diffusion controlled formation of a very fine mixture of ferrite and cementite. The formation of these phases reduces the strength of the HY-100 steel somewhat, but allows for improved toughness and ductility. During the welding process, the properties gained during heat treatment are lost, and the cooling rate of the steel must be carefully controlled to prevent the formation of martensite, particularly in the coarse grained heat affected zone (HAZ). High strength steels are particularly susceptible to weld cracking particularly when hydrogen is present; this is termed hydrogen induced cracking (HIC). HIC has three main causes: "Hydrogen in the weld metal, high stress, susceptible microstructure (martensite), and relatively low temperature (between 200 and - $100^0$ C)."[Ref.4] Hydrogen, stress, and temperature can be controlled during the welding process with strict controls on in-process fabrication procedures. In order to reduce the susceptibility of high strength steel to the formation of martensite, a high strength steel is needed which relies less on the strengthening due to carbon, and more on the strengthening achieved through alternative alloy additions.

### 2. HSLA-100

HSLA steels were developed by the US Navy to provide the same strength and toughness as HY steels, but without the inherent weldability problems due to the higher carbon content of HY-100 steels (0.13-0.17 wt.%). HSLA steels are also quenched and tempered steels which develop their strength from a combination of lath ferrite/martensite formation, solid solution strengthening, precipitation strengthening (copper), and grain size control effected through pinning of grain boundaries by niobium carbonitride during a non-recrystallization controlled final roll pass. HSLA steels are more resistant to hydrogen induced cracking in the heat affected zone due to a lower carbon content (lower carbon martensite), and thus should not require the same fabrication controls as HY-100; particularly the requirement for a preheat and a controlled interpass temperature. Fewer fabrication controls naturally result in reduced costs.

In order for HSLA steels to attain the same strengths as HY steel the addition of more alloying elements to replace the solid solution strengthening effect of carbon are required. Alloying additions must be carefully chosen; while an increase in strength may be realized by the addition of an element , it may also reduce the impact transition temperature to an unacceptable level. Figure 2-2 illustrates the effects of various elements and structural factors on the impact transition temperature. In the comparison of HY and HSLA steels (Table 2-1), the primary chemical differences lie in the increased amounts of nickel, copper, manganese, and niobium, and the lower carbon content of HSLA steels.

After carbon , manganese is considered the best alloy addition to steel to increase hardenability without sacrificing impact toughness. Niobium is added as a grain refiner (increases both strength and toughness), while copper is added to HSLA steel to provide precipitation strengthening. Nickel is added to improve toughness and as a solid solution strengthener, and the combination of nickel, manganese and copper act as austenite stabilizers.[Ref.5]

The filler wires currently in use with HSLA-100 steels meet the compositional requirements of MIL-120S. MIL-120S filler wire was designed for use with HY-100 steels and resembles the composition of HY-100, but with a somewhat reduced carbon content of about 0.07 wt. %.[Ref. 3] The higher carbon content of the filler wire (relative to the HSLA base plate) results in a cooling rate sensitive microstructure due to the higher hardenability and thus tendency to form brittle microstructures at fast cooling rates. This cooling rate sensitive weld metal requires similar in- process fabrication controls as if welding with HY-100. The objective of the current welding consumable research in the US Navy is to develop a filler wire specifically for use with HSLA-100 in the GMAW process which requires less in-process fabrication controls. To achieve this the carbon content must be significantly less than 0.07 weight percent.

## B. GAS METAL ARC WELDING (GMAW)

In the GMAW process an electric arc is established between the filler wire (acting as an electrode) and the base metal which generates temperatures high enough to melt and fuse the base and filler wire into a molten pool. Figure 2-3 illustrates typical GMAW equipment arrangement. A cover gas, typically a combination of an inert gas (argon or helium) and carbon dioxide ($CO_2$) or oxygen, is blown over the molten weld pool to prevent atmospheric contamination. Three basic types of metal transfer are employed in the GMAW process: short circuiting, spray, and globular. Short circuiting occurs when the filler wire is in contact with the base metal and will not be considered in this study. In the globular, or spray transfer method , metal drops detach from the filler wire and travel across the arc gap to be deposited in the molten base metal. The spray transfer method is typically used with direct current reverse polarity (DCRP) for steel applications. DCRP refers to the polarity of the welding equipment with the electrode being attached to the positive terminal of the welding machine. The electrode positive arrangement generates more heat at the electrode rather than at the base metal, and in GMAW is preferred as the majority of the heat generated in the welding process (approximately two thirds) is used to melt the filler wire. In gas tungsten arc welding (GTAW), the polarity is typically direct current straight polarity (DCSP) so that the majority of the heat generated in the welding process is used to melt the base metal vice the tungsten electrode. In GMAW, the composition of the shielding gas, the heat input, and the electrode size determine the method of metal transfer. [Ref. 4,6]

The GMAW welding process is preferred over the gas tungsten arc welding (GTAW), when circumstances permit, due to its deeper penetration welds, higher deposition rate and resulting reduced cost. While the depth of penetration, and rate of deposition, for GMAW is not as satisfactory as submerged arc welding (SAW), GMAW has the advantage over SAW in the fact that it is a virtually all position welding process, and SAW cannot usually be used for repair work.[Ref.6]

## C. ULTRA LOW CARBON FILLER WIRE

The primary purpose of the chemical composition of the filler wire is similar to the reason behind the microalloying of the base plate material: to ensure the mechanical properties of the weld meet required specifications by control of the final weld microstructure through the suppression of the austenite to pro-eutectoid ferrite reaction.[Ref.5] The delay of the proeutectoid ferrite reaction allows for the formation of higher strength competitive growth mechanisms (bainite and martensite). The toughness of martensite and bainite are not as good as ferrite, but in appropriate situations it can meet MIL-120S requirements. The objective of this filler wire development program is to chemically control the microstructure of the weld metal in order that the required mechanical properties can be achieved irrespective of cooling rate and thus welding heat input (power). This control is achieved by ensuring that the carbon contents of the transformation products are kept as low as possible. If the same desirable microstructure can be obtained over a wide range of cooling rates then the in-process fabrication controls needed for HY steels will not be required. Figure 2-5 illustrates a continuous cooling transformation diagram for a HSLA steel.

The large flat topped acicular ferrite (AF) and granular ferrite (GF) start curve represent an essentially bainitic microstructure over a wide range of cooling rates. Reducing the carbon content further allows a large extension of the flat topped region thus making the material less cooling rate sensitive.

A secondary purpose of elements added to the filler wire is to deoxidize the weld pool. Oxygen in the cover gas, added to stabilize the arc, will generate porosity in the weld if excess oxygen in the weld pool is not captured by deoxidizers.[Ref.7] Oxygen, as well as hardenability elements, can effect weld metal microstructure and mechanical properties. The strongest deoxidizer is aluminum, followed by titanium, silicon, and manganese. If zirconium is present this is also a very strong deoxidizer. Manganese can also react with sulfur to form MnS and, if copper is present in sufficient amounts, CuS can also form. The ability to generate MnS prevents the formation of FeS which forms liquid films at grain boundaries and can lead to hot cracking. These complex oxides, and sulfides, which are formed in the weld pool are termed non-metallic inclusions and will be discussed further in section D1.

## D. WELD METAL MICROSTRUCTURE

The International Welding Society identifies five microstructural features of HSLA weld metals in the optical microscope:

- primary ferrite (PF): includes both grain boundary ferrite and intragranular polygonal ferrite
- acicular ferrite (AF)
- ferrite with second phase (FS): includes aligned and non-aligned second phase (upper and lower bainite)
- ferrite carbide aggregate (FC): (pearlite)
- martensite (M): includes lath and twin.[Ref.8]

Primary ferrite is the initial transformation product as the weld metal cools from the austenitic range. A diffusion controlled reaction, primary ferrite is a high temperature transformation product that begins at prior austenite grain boundaries. Slower cooling rates, high weld metal oxygen contents (high inclusion density), and fine prior austenite grain size, promote the growth of primary ferrite and will result in lowering of the impact transition temperature or toughness of the weld.[Ref.9]

The most advantageous microstructure in weld metal is acicular ferrite, which can be generated when the weld metal oxygen content is of the order of 300ppm in the form of appropriate intragranular oxide inclusions, and when the prior austenite grain size is relatively large (> 45 microns).[Ref.7] In high strength steels these oxide inclusions are usually manganese alumino-silicates which contain some titanium, often as TiO. Acicular refers to the appearance of the microstructure in the optical microscope - small needle like laths finely interlocked. Acicular ferrite is believed to provide optimum weld mechanical properties in both strength and toughness by providing a fine interlocking microstructure which hinders crack propagation.[Ref.9] Acicular ferrite can often be found in GMAW welds if cooling rates and oxygen contents are appropriate.

As the weld pool begins to cool below $600^0$ C, the thermodynamic driving force behind the transformation of austenite begins to increase, and intragranularly nucleated phases (acicular ferrite) become more favored. As the austenite begins to decompose into ferrite, carbon is being rejected form the ferrite into the adjoining austenite. This carbon enrichment of the austenite suppresses ferrite formation in these areas and can lead to the formation of ferrite with a second phase (bainite). With low intragranular inclusion density, the ferrite growth from the grain boundary continues relatively unimpeded and results in large aspect ratios (10:1) with interspersed carbide particles or ferrite carbide aggregate (pearlite).[Ref.8]

Martensite is an extremely strong and brittle microstructure. Martensite is formed when the cooling rate is fast enough (< 5s from 800 to $500^0$ C) prevent the diffusion controlled reactions from starting.[Ref.5] A low temperature, combined with a large thermodynamic driving force for the decomposition of austenite, results in martensite. Martensite may also become trapped between ferrite laths, resulting in martensite islands in the microstructure due to the carbon enrichment of the austenite and a rapid cooling rate.

The micro-constituents present in the final weld microstructure formed is dependent on the interaction of the following variables:

- total alloy content (base metal and filler wire)
- the size, chemical composition, and distribution of non-metallic inclusions
- the solidification microstructure
- the prior austenite grain size
- the weld power (heat input), and therefore the weld thermal cycle or cooling rate during the transformation of metastable austenite.[Ref.5]

### 1. Non-Metallic Inclusions

Inclusions are formed by the interaction of oxygen in the cover gas with the iron alloying agents in the weld pool. These oxide, or oxy-sulfide inclusions in some cases, float to the surface and form slag, but more frequently are trapped by the rapid solidification process in the weld pool. The formation of the weld metal oxides is a complex thermal process, but can be simplified by a two stage model:

- a high temperature portion, where some reactions are near equilibrium, and
- a cooling stage where the concentrations established during the high temperature stage are adjusted by the precipitation of new phases.

The high temperature portion of the model represents the area from the arc tip to the molten pool below the arc gap. The temperature range of the high temperature stage is $1600\text{-}2400^0$ C. The cooling stage covers the period of time from after the passage of the arc tip and is characterized by the deoxidation reactions [Ref.5].

There are three primary sources for the inclusions in steel: primary, secondary and exogenous. Primary inclusions are generated before weld pool solidification, and secondary inclusions are formed form in the supersaturated regions of the interdendritic melt. Exogenous inclusions are formed from outside the melt. The composition and role of inclusions in the manufacture of steel plate are well understood, and microstructure and mechanical properties can be reasonably well predicted. Steel manufacturing data cannot predict weld metal results as the rapid weld pool cooling process precludes attainment of an equilibrium condition.[Ref. 10,11] The nature, and chemical composition of inclusions in weld metal is currently an intense area of study since appropriate inclusions promote the development of acicular ferrite within the solidified weld metal [Ref.10]

### 2. Characterization of Inclusions in High Strength Steel Weld Metal

Inclusion phases and compositions are analyzed in the transmission electron microscope (TEM) by energy dispersive x-ray (EDX) microanalysis, and electron energy loss spectroscopy (EELS), and diffraction . When a high energy electron impacts an atom and removes an electron, an electron from an outer shell drops down to fill the hole generated by the removal. The difference in the energies of the removed and outer shell electrons can be made up in two ways:

- emission of a photon (x-ray) whose energy is characteristic of the atom, or
- by ejecting a nearby electron (Auger electron).[Ref.20]

The ratio of photons to Auger electrons emitted is termed fluorescent yield (ω) and is characteristic of the atom and electron shells involved. EDX microanalysis consists of hitting inclusions with high energy electrons (e.g. 200kV) in a transmission electron microscope (TEM) and measuring the intensity of the characteristic x-rays emitted from the specimens. An EDX spectrum provides a plot of x-ray intensity vs. energy of characteristic emissions. EELS measures the energy losses of the high energy electrons as they passes through the inclusion. EELS losses include the characteristic x-ray as well as the ejected Auger electrons. An EELS spectra provides a plot of intensity vs. energy loss. One advantage of EELS analysis is that the detection of light elements is much improved. Light element x-rays are typically absorbed by the EDX detector windows and the efficiency of generation of x-rays for light elements is poor. EELS spectra also provide the capability to determine not only the concentration of the phases present, but can also give information on the way the elements are bonded in these phases.

TEM EDX analysis is considered superior to scanning electron microscope (SEM) analysis of inclusions and was used in this study. SEM EDX analysis is not considered optimum in that the generation of electrons and x-rays from the sample is in the shape of a bulb which penetrates approximately 2μm into the sample.[Ref.20] Figure 2-6 graphically illustrates the bulb of interaction. As the typical weld pool inclusion is approximately 0.4μm in diameter, the SEM plus EDX results include components of the base metal which cannot be separated from the inclusion data.

For TEM analysis, inclusions are removed from the base metal by a carbon replica technique. A thin foil of the carbon coating and the removed inclusion is placed on a 3mm copper grid and then analyzed in the TEM. TEM analysis of inclusions result in a thin foil approximation which avoids the base metal contamination of SEM EDX analysis. The x-ray measured intensity is a function of the following:

$$I_A = iQ\omega n \tag{2.1}$$

where,

$I_A$ = the intensity generated by element A
$i$ = the current incident on the inclusion

$Q$ = the cross section per $cm^2$ for the ionization event
$\omega$= fluorescent yield
n= the number of atoms in the excited volume.[Ref. 20]

In an element composed of elements a and b, the ratio of

$$n_a / n_b = \frac{I_A Q_B \omega_B a_B}{I_B Q_A \omega_A a_A} \frac{\eta_B}{\eta_A} \tag{2.2}$$

where,

$a_A$ = fraction of K,L,M line collected, and
$\eta_A$ =detector efficiency,

is the basis for microanalysis of inclusions.[Ref.20] With a measured intensity value for each element, the number of atoms of each element present can be easily calculated. The ratio of the number of atoms of a and b can provide the concentration of elements present in inclusions. For specimens that are too thick for the thin foil approximations, a correction must be made for the absorption of the x-ray energies as they leave the specimen. Absorption corrections were made in this study as appropriate [Ref. 20].

Research to date indicates that the inclusions in high strength steel weld metal contain several different compounds which vary in composition depending on the welding conditions (heat input/cooling rate), the total alloy content (base metal and filler wire), and the cover gas, or flux, in use. Previous research by many workers has indicated that these inclusions contain MnO, $SiO_2$, $Al_2O_3$, and usually a titanium oxide (often TiO),as well as CuS and MnS.[Ref. 5,8,9,10,12,13] These multi-phase inclusions are typically spherical particles, but often have angular facets in the titanium rich areas. The equilibrium ternary phase diagram illustrated in Figure 2-7 details the coexisting compositions and compounds of the system $Al_2O_3$ - MnO - $SiO_2$ . While this ternary is a good approximation of the phases present in inclusions it has several shortcomings. First, the ternary describes an equilibrium state and the formation of inclusions is not an equilibrium process due to the rapid cooling rate within the weld pool. Second, most inclusions analyzed have a definite titanium concentration which is not represented in this ternary. To include titanium would result in a $Al_2O_3$-TiO- MnO or $Al_2O_3$-TiO- MnO-$SiO_2$ quartenary diagrams, which were not identified after literature searches by Dowling et al.-and are not yet apparently available [Ref.10]

The composition and distribution of non-metallic inclusions are of interest in welding research due to their roll in transformation kinetics. Inclusions promote the growth of acicular ferrite and thus contribute to the improved mechanical properties of the weld metal.

### 3. Transformation Kinetics

Solid state transformations occur heterogeneously at the most energetically favorable sites. These high energy sites are grain boundaries, grain corners, inclusions, dislocations, and vacancy clusters. In weld metal transformations the non-metallic inclusions provide sites to promote the energetically favorable heterogeneous nucleation. Research performed by Ricks et al., indicates that the nucleation of ferrite at inclusions is always energetically more favorable than homogeneous nucleation, but less favorable than nucleation at austenite grain boundaries. [Ref.14] The most favorable nucleation sites were found to be particles of radius 0.2-0.5μm. This range of particle size is the most prevalent for non-metallic inclusions in many steel weldments. Ricks et al., did not consider the effects of strain caused by the different thermal properties existing between the austenite and the inclusions, or the possibility of the ferrite to adopt favorable orientations with the austenite and the inclusions. Grong et al., considered these oversights to strongly influence the transformation process, and may explain why certain types of inclusions (composition and shape) may be excellent nucleation sites for acicular ferrite.[Ref. 5]

On cooling below the $Ac_3$ temperature, ferrite will nucleate initially at the austenite grain boundaries and begin to form allotriomorphs. As the degree of under-cooling increases the diffusion controlled transformations begin to slow down and the formation of displacive mechanisms begin to control the transformation. The cooling time between 800-500$^0$C is considered the critical range for the austenite to ferrite transformation. The cooling time from 800-500$^0$C is proportional to the heat input and may be approximated by the following formula:

$$\Delta t_{8/5} \cong 5\eta E \tag{2.3}$$

where, η = the arc efficiency (0.65-0.85 for GMAW), and E= the heat input [kJ/mm].[Ref. 5] The alloys in the filler wire chemically suppress the ferrite grain boundary transformation until the degree of undercooling will allow intergranular nucleation of acicular ferrite and displacive phases (bainite/martensite) in the weld metal. The initial solidification of the weld structure takes place epitaxially, where the partly melted base metal grains at the fusion boundary act as seed crystals for the columnar grains. The growth of the grains continues in the direction of the maximum thermal gradient in the weld pool. In order to prevent this coarse columnar structure from dominating the microstructure, and providing propagation paths for cracks, the number and size of non-metallic inclusions again plays a dominant role. The heterogeneous nucleation of new grain structure ahead of the solidification front is dependent on the non-metallic inclusions. Figure 2-5 illustrates the ideal continuous cooling transformation curve in that the bainitic microstructures (AF and GF) will be realized over a wide range of cooling rates. A low cooling rate (high heat input) will produce Widmanstätten and polygonal ferrite, and a rapid cooling rate will generate a martensitic structure.[Ref. 5,15] The best mechanical properties of strength and toughness are obtained with the acicular microstructures. In order to obtain an acicular vice a granular microstructure, the inclusion size and volume fraction must be optimized to provide sufficient intragranular nucleation sites. The size and volume fraction of inclusions both increase with increasing weld metal oxygen [Ref. 16]. These results suggest that optimizing the weld metal oxygen activity and total alloy content will have definite role in the final microstructure. Work to date on high strength steel (such as HY-100)indicates an oxygen content of ~250ppm with average inclusion size ~0.04 μm is optimum for acicular ferrite formation provided the cooling rate $\Delta t_{800\text{-}500}$ is about 15 seconds.[Ref.28]

## E. MECHANICAL PROPERTIES

An analysis of the mechanical properties of materials can reveal important information on the lattice structure and imperfections in materials. In this study, the strength (yield) and the toughness (impact transition temperature) of the as-solidified welds are of primary concern. The yield strength of a material represents the stress level at which plastic deformation of a material begins. The magnitude of yield strength represents the weld metal resistance to plastic deformation, and is a function of strength and hardness. The toughness of a weld metal refers to the ability of the metal to absorb energy up to fracture, and is a function of strength and ductility. A Charpy V-notch (CVN) test is usually used to measure the impact toughness of weld metals under a dynamic, tri-axial stress state through a range of temperatures. Steels, or body centered cubic (BCC) structures are particularly susceptible to a significant decrease in toughness at low temperatures, and in order to ensure the satisfactory service of weld metals through an entire range of possible temperatures, the Charpy V-notch test is utilized.

The factors affecting the CVN toughness of ultra low carbon weld metals are the strength, the size and distribution of non-metallic inclusions, and the final solidified microstructure.[Ref.17] Increasing strength and carbon content lead to reduced toughness. Higher carbon content metals tend form harder and more brittle microstructures. The increased carbon content results in a greater percentage of carbide aggregates in the weld metal. These carbide aggregates form in the carbon enriched areas adjacent to ferrite laths and provide a brittle crack propagation path.[Ref.3,17]. Strength is a function of the final microstructure formed in the weld metal with martensite being the strongest structure formed, but also the least ductile [Ref.3,17].

The size and distribution of inclusions are important in that as the total volume fraction of inclusions increases, the CVN upper shelf energy decreases as a power function.[Ref.17] The reasoning behind this is that large inclusions strain the surrounding microstructure and provide excellent initiation sites for cracking and micro-void coalescence. Inclusions also play a role in decreasing the amount of columnar grains present in the final solidified weld.

Columnar grains typically form in GMAW welds in the final solidified microstructure due to the relatively fast cooling rate (5-10sec) and limited number of passes.[Ref. 5] These columnar grains provide excellent crack propagation paths and are an impediment to toughness and impact strength. Good impact properties typically depend on a fine, interlocking , microstructure to prevent crack propagation. Acicular ferrite is generally believed to be the optimum final microstructure to provide the best impact properties. However, the ultra low carbon weld metals previously studied (both GMAW and GTAW) have very low (10-15%) or no acicular ferrite present respectively, and provide excellent impact properties and transition temperatures.[Ref.17] The low acicular ferrite percentages of GMAW and GTAW welds combined with excellent toughness suggests that acicular ferrite does not appear to be a major contributing factor to the toughness of the ultra low carbon welds studied so far.

Improvement in impact properties (toughness) can be achieved through decreasing strength, carbon content, nitrogen content, inclusion size and volume fraction, and the amount of columnar solidified structure. When these complex factors can be optimized, toughness equivalent to tempered martensite may be realized in steel weld metal.[Ref. 17] The focus of this study is to examine the factors affecting the impact toughness of GMAW ultra low carbon welds.

| Element | HY-100 | HSLA-100 | Filler Wire |
|---|---|---|---|
| C | 0.17 | 0.034 | 0.03 |
| Mn | 0.25 | 1.18 | 1.51 |
| P | 0.01 | 0.008 | < 0.004 |
| S | 0.005 | 0.002 | 0.002 |
| Si | 0.25 | 0.25 | 0.35 |
| Cr | 1.40 | 0.047 | 0.009 |
| Ni | 2.90 | 3.51 | 4.95 |
| Mo | 0.40 | 0.18 | 0.54 |
| Cu | 0.05 | 1.25 | 0.003 |
| Nb | --- | 0.039 | < 0.002 |
| V | 0.01 | 0.001 | 0.002 |
| C.E. | 0.81 | 0.64 | 0.78 |

CE= Carbon Equivalent

$$CE = C + \frac{Mn + Si}{6} + \frac{Ni + Cu}{15} + \frac{Cr + Mo + V}{5}$$

Table 2-1 Chemical Composition of HY-100, HSLA-100, and Filler Wire

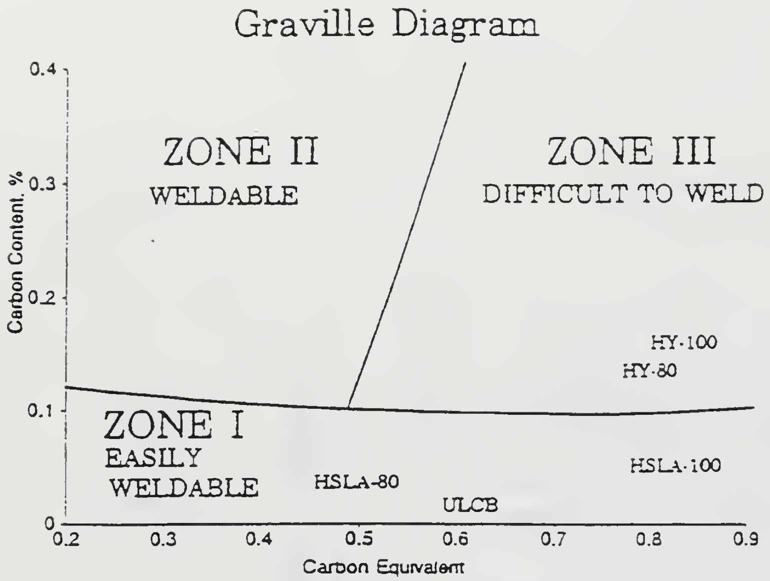

$$C.E. = C + \frac{Mn + Si}{6} + \frac{Ni + Cu}{15} + \frac{Cr + Mo + V}{5}$$

Figure 2-1 Graville Diagram [from Ref. 19]

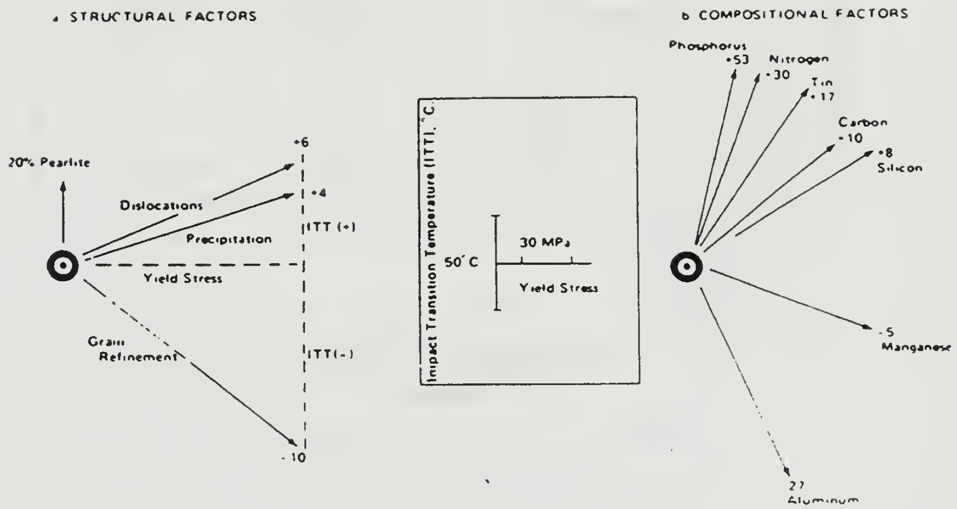
a STRUCTURAL FACTORS
20% Pearlite
Dislocations
Precipitation
Yield Stress
Grain Refinement
+6
+4
ITT (+)
ITT (-)
-10
Impact Transition Temperature (ITT), °C
50°C
30 MPa
Yield Stress
b COMPOSITIONAL FACTORS
Phosphorus
+53
Nitrogen
+30
Tin
+17
Carbon
-10
+8
Silicon
-5
Manganese
27
Aluminum

Figure 2-2 Factors Affecting the Yield Stress and Impact Transition Temperature in Ferrite-Pearlite Steels [from Ref. 18]

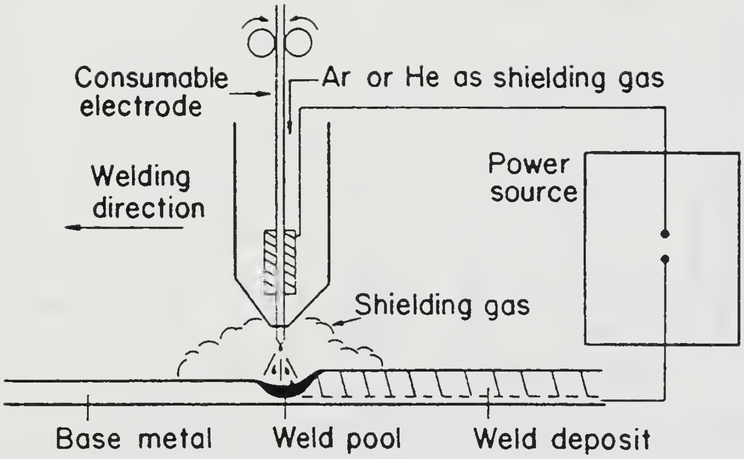
Consumable electrode
Ar or He as shielding gas
Welding direction
Power source
Shielding gas
Base metal
Weld pool
Weld deposit

Figure 2-3 Schematic of the Gas Metal Arc Welding Process (GMAW) [from Ref.4]

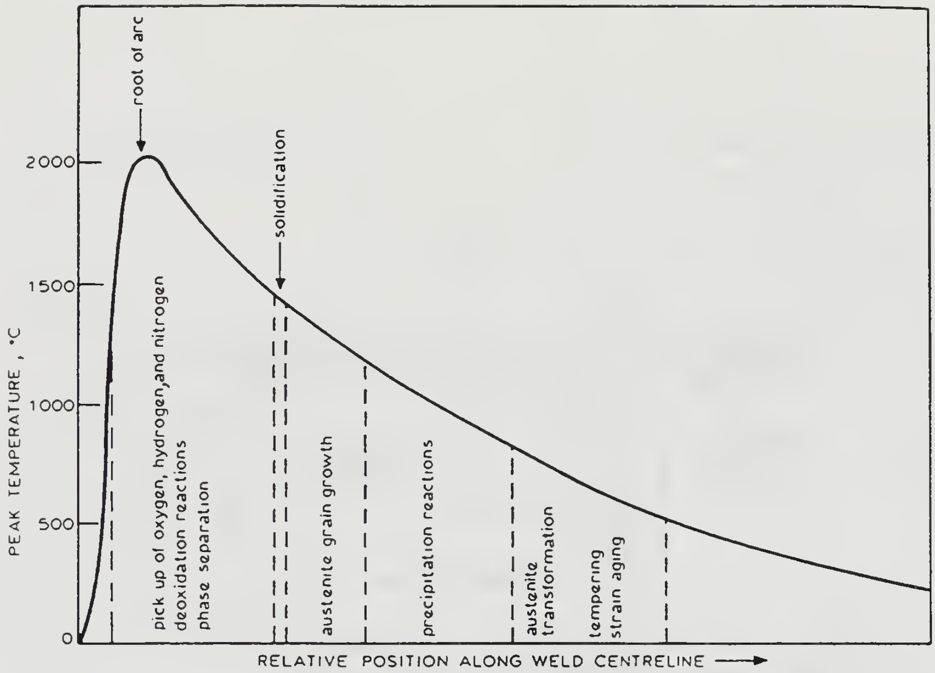

Schematic diagram illustrating weld centreline peak temperature at different distances from root of arc: characteristic temperature ranges where specific chemical and physical reactions occur during cooling of weld metal down to room temperature are also included

Figure 2-4 Weld Pool Thermal Profile [from Ref. 5]

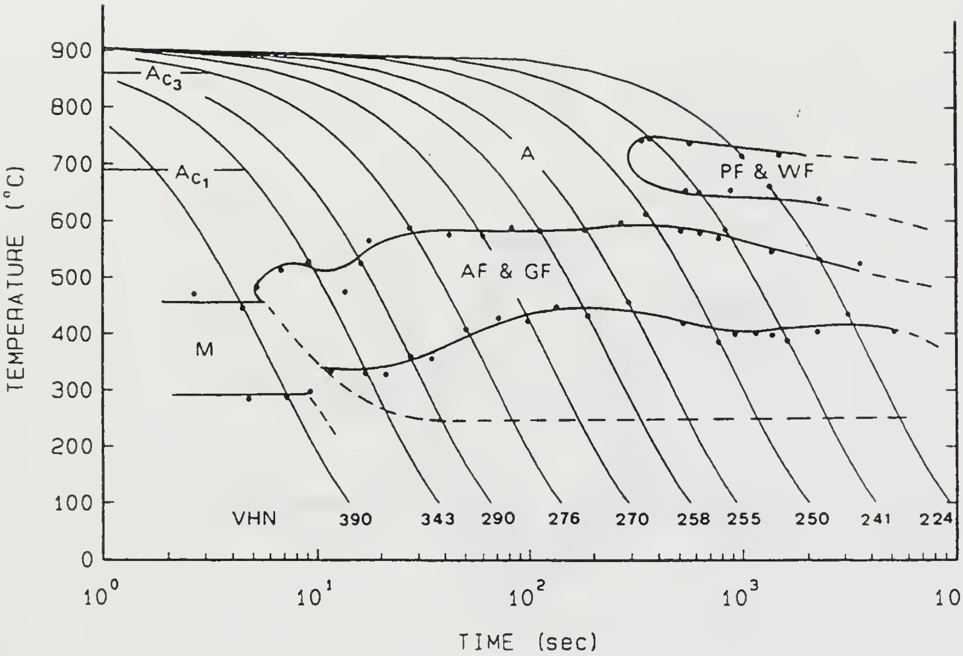

Figure 2-5 Representative Continuous Cooling Diagram for Low-Carbon HSLA Steel

[from Ref. 15]

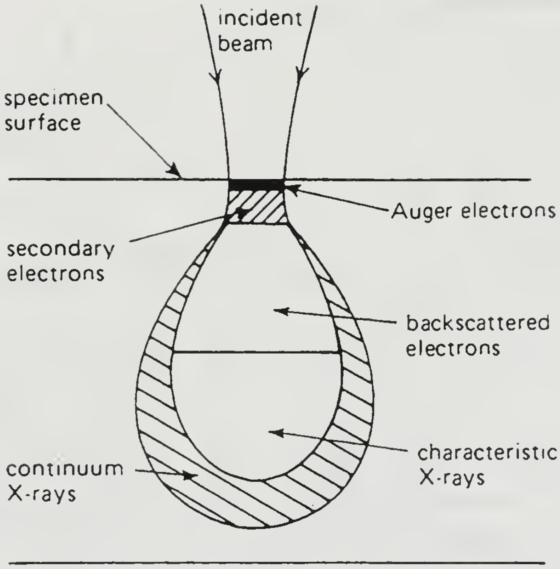
incident
beam
specimen
surface
Auger electrons
secondary
electrons
backscattered
electrons
characteristic
X-rays
continuum
X-rays

Figure 2-6 Schematic Diagram of the SEM Bulb of Interaction [from Ref. 20]

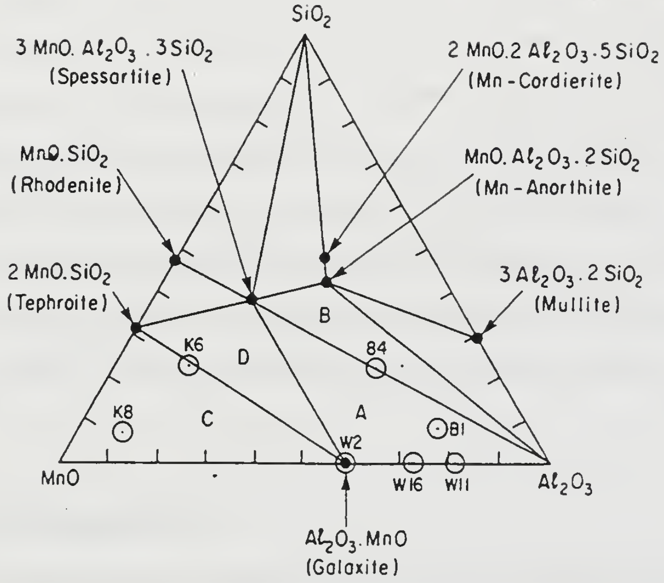
SiO2
3 MnO. Aℓ2O3 . 3SiO2
(Spessartite)
2 MnO.2 Aℓ2 O3 .5 SiO2
(Mn-Cordierite)
MnO.SiO2
(Rhodenite)
MnO. Aℓ2 O3 . 2 SiO2
(Mn-Anorthite)
2 MnO.SiO2
(Tephroite)
3 Aℓ2O3 . 2 SiO2
(Mullite)
B
K6
D
84
K8
C
A
81
W2
MnO
W16
W11
Aℓ2O3
Aℓ2O3.MnO
(Galaxite)

Figure 2-7 Ternary Diagram of Coexisting Phases in Annealed Mixes for the System $Al_2O_3$-MnO-$SiO_2$ [from Ref. 10]

# III. EXPERIMENTAL PROCEDURE

## A. WELD SAMPLES

One Charpy impact specimen (MV14) and three weld samples (JB32, JB33, JB34) were forwarded from Naval Surface Warfare Center (NSWC), Bethesda, Maryland for analysis. All welds, including MV14, were fabricated by GMAW process using 51 mm thick HSLA-100 steel for the base plate material and an ultra low carbon steel filler wire. The filler wire was 1.6 mm square in cross section and was manufactured by successive rolling (with intermittent vacuum annealing) from 19 mm square cross sections removed from ingots of experimental ultra low carbon steel plate material. Welding parameters are shown in Table 3-1. All welds, including MV14, were 16 mm deep with a $60^\circ$ included angle single V. Weld samples were removed with a transverse orientation to the direction of weld travel. The Charpy sample was also removed from the weld in a transverse orientation with the V-notch aligned in the center of the fusion zone. Weld sample chemical analysis were taken from the middle of the fusion zone (same position as Charpy samples). The method and precision of chemical analysis were as reported in Table 3-2.

## B. SAMPLE PREPARATION

All weld samples were ground using 180, 240, 320, 400, 600, and 800 grit silicon carbide paper, followed by final polishing with 3μm water based diamond on Beuhler Texmet 1000 and 0.05μm alumina on Beuhler Microcloth. All samples were ground and polished using the Beuhler Ecomet 4 with Automet 2 Power Head.

## C. SCANNING ELECTRON MICROSCOPY

Polished weld samples were placed in the Cambridge Stereoscan 200 scanning electron microscope ( SEM) for inclusion size and volume fraction analysis. For improved resolution and contrast, the SEM was operated in the backscatter mode. One hundred random fields were selected for analysis from the fusion zone of all weld samples. All inclusion measurements and counts were taken with the SEM $LaB_6$ filament energized to 20 kV, a 9mm working distance and at magnification 4000X. Figure 3-1 illustrates a typical inclusion field and method of inclusion diameter measurement. The inclusion field size was $510.6 \times 10^{-12}$ $m^2$ for all measurements. Figures 3-2 through 3-5 illustrate inclusion histograms, mean diameter, and volume fraction measurements for each sample.

Inclusion volume fraction was calculated from mean diameter data using the following formula:

$$VolFr = \frac{s}{f} \times \pi \frac{d^2}{4} \tag{3.1}$$

s = Average # inclusions / field

f = inclusion field size ( $510.6 \times 10^{-12}$ $m^2$ )

d = inclusion mean diameter

The area fraction and volume fraction can be considered as equivalent with the following assumption:

- The plane of polish analyzed has the same probability of any other plane as having equivalent inclusion statistics.[Ref.21]

Table 3-3 lists a summary of inclusion statistics.

Two Charpy bars were returned by NSWC for fractographic analysis in the SEM. One upper shelf and one lower shelf sample from MV14 were photographed and analyzed in the secondary electron mode of the SEM (20kV) at various magnifications to determine the mechanism of failure.

## D. TRANSMISSION ELECTRON MICROSCOPY

The TOPCON 002B transmission electron microscope (TEM) with $LaB_6$ filament energized to 200kV was utilized for energy dispersive x-ray (EDX) analysis of twenty randomly chosen inclusions. TEM samples were prepared from polished weld samples that had been etched in a solution of 5% Nitric acid and 95% Methanol (Nital) for 25 seconds. Etched samples were then carbon coated using an Ernest F. Fullam Mk II carbon coater. Two strands of carbon fiber were utilized to coat the samples which were approximately 3.20 cm from the filament. Coated samples were then scribed in several 3 mm squares in the fusion zone of each weld to promote separation upon deep etching. Samples were then deep etched in Nital for approximately 5 minutes until the carbon coating began to float off. The carbon coating and attached inclusions were placed into a 5% by volume solution of acetone and water. The surface tension of the acetone and water solution flattened out the carbon replica so that it could be placed on a 400 mesh copper TEM grid. TEM samples for analysis were tilted 10 degrees toward the EDX detector for improved results. The Topcon TEM uses a super ultra thin window for improved detection of light elements. EDX data was analyzed using EDAX/EDX software. Figures 3-6 through 3-9 illustrate typical EDX spectra obtained for each sample, and Tables 3-4 through 3-7 report inclusion chemical analysis results.

In addition, confirmation of EDX results was obtained through the parallel electron energy loss spectrum (PEELS) analysis of several thin inclusions. A typical PEELS spectrum is illustrated in Figure 3-10.

Samples for TEM microstructural analysis were cut from the Charpy sample fusion zone of MV14 using a high speed diamond saw in 1mm thick slices. Samples were then mechanically thinned by hand using 400, 600, and 800 grit silicon carbide paper. Three millimeter disks were punched out of the thinned sample and twin-jet electro-polished in a solution of 3% Perchloric acid, 35% Butanol, and 62% Ethanol at $-50^0$ C until a small hole developed. The E.A. Fischione Instrument, Mfg., twin-jet electropolisher was utilized with settings of 75 volts and 5 milli-amps.

## E. OPTICAL MICROSCOPY

The Zeiss Stereomicroscope was utilized to obtain type 667 Polaroid film photographs of the MV-14 Charpy fracture surfaces. The upper and lower shelf fracture surfaces of MV-14 are illustrated in Figure 3-11. After polished weld samples were etched for 6 seconds, the Zeiss Jenaphot 2000 optical photomicroscope with attached 35mm camera was used to obtain representative pictures of the fusion zone microstructure. Figures 3-12 through 3-15 represent typical fusion zone microstructure for all samples. The percentage of acicular ferrite in the weld metal was determined by taking ten random photos (type 667 Polaroid film) in the fusion zone and then superimposing an approximately 1.27cm rectangular grid pattern, resulting in 48 grid points per photo. This technique resulted in 480 grid points per sample for microstructural analysis. Figures 3-16 and 3-17 illustrate representative photos used for AF percentage analysis. As explained in previous work (Clark), ASTM standard E 562-89 was used as a guide in the determination of percentage of phases present, but was not followed in the area of the recommended number of grid points per volume fraction being analyzed, or in the area of statistical analysis.[Ref.22,23] The following binomial approximation was utilized vice ASTM standard E 562-89 :

$$\sigma^2 = p(1-p)/n \tag{3.2}$$

where, σ = standard deviation

p = proportion of phases being analyzed

n = number of grid points.[Ref.24]

Table 3-8 reports the AF phase percentages and standard deviation calculated for all weld samples.

The Zeiss stereomicroscope was used to take macrograph photos of the weld at 8x. Photos were then digitized by Semicaps capture software and stored on floptical disks. Printed photographs were then pieced together in a montage. The completed montage was then photographed on Polaroid 35mm film for a final magnification of approximately 3x.

## F. MICROHARDNESS MEASUREMENTS

Microhardness measurements were made using the Beuhler Micromet 2004 with a one kilogram load and diamond pyramid indenter. Polished samples were etched for 6 seconds in Nital prior to indentation to ensure all measurements were taken in the fusion zone. Ten randomly chosen indentations were made in the center of the fusion zone (same location as the Charpy bars V-notch). All results are reported in Table 3-9 using the Vickers scale.

## G. MECHANICAL TESTING

NSWC conducted all Charpy V-notch tests and determined resulting FATT temperatures. After converting hardness data from the Vickers to the Brinell scale, specimen tensile strengths were calculated using the following formula:

$$S_U = 0.45H_B \tag{3.3}$$

where,

$S_U$ = Ultimate Tensile Strength [ksi]

$H_B$ = Brinell Hardness.[Ref.25]

Weld sample yield strengths were calculated from tensile strength results using the following approximation based on considerable amounts of previous work at the Naval Postgraduate School:

$$S_Y = S_U(0.9) \tag{3.4}$$

where,

$S_Y$ = Yield Strength.[Ref.19,22]

Tensile and yield strength data are reported in Table 3-10. NSWC conducted tensile and yield strength tests of MV14 (pull tests) and obtained data comparable to calculated values ($S_U$ = 126 ksi; $S_Y$ = 105 ksi).

## H. ERROR

Error bars on all data plots represent 95% confidence intervals for either large (n>30) or small (n<30) sample size using the following formulas respectively [Ref. 26]:

$$\mu = \bar{x} \pm z_{c/2}\frac{S_x}{\sqrt{n}} \tag{3.5}$$

$$\mu = \bar{x} \pm t_{\alpha,\upsilon}\frac{S_x}{\sqrt{n}} \tag{3.6}$$

where,

$\mu$ = true mean value
$\bar{x}$ = calculated mean value
z =distribution, large sample size
c = confidence interval
$S_x$ = standard deviation
n = sample size
$\alpha$ = 1 - c
$\nu$ = (1 - n) degrees of freedom
t = distribution, small sample size.

| SAMPLE | WELD TYPE / # PASSES | COVER GAS | POWER [KJ/IN] | VOLTAGE | CURRENT [AMPS] | TRAVEL SPEED [IN/MIN] |
|---|---|---|---|---|---|---|
| MV14-9 | GMAW / 7 | 95% Ar - 5% $CO_2$ | 62 | 28.4 | 311 - 317 | 8.5 |
| JB-32 | GMAW / 8 | 98% Ar - 2% $O_2$ | 60 | 27 | 320 - 340 | 8.4 - 8.9 |
| JB-33 | GMAW / 8 | 95% Ar - 5% $O_2$ | 60 | 26.9 - 27.4 | 340 | 8.9 |
| JB-34 | GMAW / 8 | 90% Ar - 10% $O_2$ | 60 | 26.9 - 27.4 | 340 | 8.9 |

Table 3-1 Weld Parameters

| Element | Analysis Method | Confidence Limit +/- (wt %) |
|---|---|---|
| **Carbon** | Combustion Infrared | 0.001 |
| **Manganese** | Plasma Emission | 0.02 |
| **Silicon** | Plasma Emission | 0.01 |
| **Phosphorus** | Plasma Emission | 0.002 |
| **Sulfur** | Combustion Automatic Titration | 0.001 |
| **Nickel** | Plasma Emission | 0.05 |
| **Molybdenum** | Plasma Emission | 0.01 |
| **Chromium** | Plasma Emission | 0.02 |
| **Vanadium** | Plasma Emission | 0.001 |
| **Aluminum** | Plasma Emission | 0.002 |
| **Titanium** | Plasma Emission | 0.001 |
| **Zirconium** | Plasma Emission | 0.001 |
| **Copper** | Plasma Emission | 0.001 |
| **Oxygen** | Inert Gas Fusion, TC 136 | 0.001 |
| **Nitrogen** | Inert Gas Fusion, TC 136 | 0.001 |
| **Boron** | Plasma Emission | 0.001 |
| **Hydrogen** | Vacuum Hot Extraction | 0.00001 |
| **Niobium** | Plasma Emission | 0.001 |

Table 3-2 Method of Chemical Analysis and Precision [from Ref. 19 ]

| Sample ID | Total Count | Mean Diameter [microns] | Std Dev [microns] | Volume fraction [%] |
|---|---|---|---|---|
| MV14 | 526 | 0.4818 ± 0.0392 | 0.34871 | 0.188 ± 0.005828 |
| JB32 | 589 | 0.4397 ± 0.0317 | 0.29877 | 0.175 ± 0.004375 |
| JB33 | 525 | 0.5208 ± 0.0369 | 0.32757 | 0.219 ± 0.006789 |
| JB34 | 364 | 0.8575 ± 0.0759 | 0.56227 | 0.412 ± 0.03003 |

Table 3-3 Summary of Inclusion Statistics

| Al [at.%] | Si [at.%] | S [at.%] | Ti [at.%] | Mn [at.%] |
|---|---|---|---|---|
| 36.7 | 13.6 | 5.0 | 8.9 | 35.8 |
| 35.4 | 17.2 | 2.3 | 13.6 | 31.5 |
| 33.4 | 14.7 | 8.9 | 11.6 | 31.2 |
| 35.6 | 16.1 | 1.9 | 13.7 | 32.7 |
| 32.1 | 18.9 | 1.9 | 13.4 | 33.7 |
| 36.8 | 19.3 | 1.3 | 10.5 | 32.2 |
| 43.1 | 14.5 | 1.5 | 12.5 | 28.4 |
| 38.6 | 19.4 | 1.1 | 12.2 | 28.7 |
| 41.9 | 14.8 | 2.6 | 10.3 | 30.4 |
| 39.3 | 16.5 | 1.6 | 11.5 | 31.1 |
| 42.1 | 15.8 | 0.5 | 10.6 | 31.0 |
| 42.2 | 13.3 | 3.2 | 10.7 | 30.6 |
| 29.0 | 25.5 | 2.1 | 10.0 | 33.4 |
| 31.2 | 16.9 | 3.3 | 12.5 | 36.0 |
| 38.1 | 12.5 | 6.3 | 12.3 | 30.8 |
| 33.6 | 16.4 | 4.6 | 11.7 | 33.7 |
| 37.2 | 14.4 | 4.7 | 12.9 | 30.9 |
| 27.5 | 27.5 | 1.8 | 8.4 | 34.9 |
| 31.3 | 18.4 | 3.3 | 13.1 | 33.8 |

Average:

| | | | | |
|---|---|---|---|---|
| 36.06 | 17.14 | 3.05 | 11.60 | 32.15 |

Note: Data represents the EDX analysis (TEM 200kV) of twenty randomly chosen inclusions

Table 3-4 MV14 Inclusion Chemical Analysis

| Al [at.%] | Si [at.%] | S [at.%] | Ti [at.%] | Mn [at.%] |
|---|---|---|---|---|
| 4.6 | 27.4 | 10.5 | 20.9 | 36.5 |
| 4.7 | 25.3 | 5.2 | 20.2 | 44.6 |
| 3.1 | 30.6 | 3.6 | 16.9 | 45.8 |
| 5.4 | 29.0 | 3.0 | 18.2 | 44.4 |
| 4.0 | 30.3 | 2.8 | 21.9 | 41.0 |
| 11.7 | 29.6 | 2.2 | 16.3 | 40.2 |
| 11.7 | 28.5 | 0.9 | 18.4 | 40.5 |
| 9.8 | 29.1 | 1.9 | 17.0 | 42.3 |
| 9.6 | 30.0 | 6.6 | 18.4 | 35.4 |
| 12.5 | 29.5 | 4.2 | 18.3 | 35.4 |
| 11.0 | 29.4 | 2.2 | 15.6 | 41.7 |
| 5.0 | 26.8 | 5.5 | 23.7 | 39.2 |
| 9.2 | 34.4 | 15.9 | 2.70 | 37.8 |
| 10.8 | 26.8 | 5.7 | 19.8 | 37.0 |
| 13.1 | 27.0 | 6.5 | 18.9 | 34.5 |
| 7.4 | 26.9 | 2.8 | 18.7 | 44.2 |
| 11.1 | 26.0 | 6.3 | 18.9 | 37.7 |
| 11.9 | 32.8 | 2.0 | 14.1 | 39.2 |
| 12.5 | 31.3 | 5.3 | 15.4 | 35.6 |
| 9.4 | 30.7 | 4.0 | 16.0 | 39.8 |
| Average: | | | | |
| 8.93 | 29.07 | 4.86 | 17.52 | 39.64 |

Note: Data represents the EDX analysis (TEM 200kV) of twenty randomly chosen inclusions.

Table 3-5 JB32 Inclusion Chemical Analysis

| Al [at. %] | Si [at.%] | S [at.%] | Ti [at. %] | Mn [at.%] |
|---|---|---|---|---|
| 1.6 | 37.0 | 3.0 | 8.9 | 49.5 |
| 1.9 | 39.2 | 3.6 | 11.8 | 43.6 |
| 2.5 | 39.9 | 3 | 3.6 | 51.0 |
| 1.8 | 39.5 | 4.0 | 5.6 | 49.0 |
| 1.9 | 29.6 | 3.5 | 14.2 | 50.8 |
| 2.3 | 37.8 | 3.3 | 8.5 | 48.1 |
| 2.0 | 37.0 | 3.2 | 8.6 | 49.2 |
| 2.4 | 34.0 | 1.8 | 11.3 | 50.4 |
| 2.5 | 35.3 | 2.6 | 10.2 | 49.5 |
| 3.0 | 32.3 | 2.5 | 13.8 | 48.4 |
| 2.2 | 32.5 | 4.6 | 17.2 | 43.4 |
| 2.8 | 29.6 | 3.5 | 17.2 | 47.0 |
| 1.8 | 39.8 | 4.6 | 5.6 | 48.2 |
| 2.4 | 39.2 | 3.4 | 11.6 | 43.5 |
| 4.6 | 40.2 | 2.7 | 3.9 | 48.5 |
| 2.0 | 38.3 | 4.3 | 9.9 | 45.6 |
| 1.8 | 37.4 | 3.9 | 9.4 | 47.5 |
| 1.6 | 38.4 | 4.2 | 7.0 | 48.8 |
| 1.7 | 37.6 | 5.4 | 6.8 | 48.5 |
| 1.9 | 39.6 | 4.2 | 7.2 | 47.1 |
| Average: | | | | |
| 2.24 | 36.71 | 3.57 | 9.62 | 47.88 |

Note: Data represents EDX analysis (TEM 200kV) of twenty randomly chosen inclusions

Table 3-6 JB33 Inclusion Chemical Analysis

| Al [at.%] | Si [at.%] | S [at.%] | Ti [at.%] | Mn [at.%] |
|---|---|---|---|---|
| 10.2 | 38.9 | 2.8 | 5.0 | 43.1 |
| 6.4 | 36.4 | 3.5 | 5.7 | 48.0 |
| 9.8 | 38.3 | 3.2 | 6.1 | 42.6 |
| 7.0 | 35.6 | 1.8 | 7.8 | 47.9 |
| 10.5 | 34.8 | 1.7 | 8.2 | 44.7 |
| 7.6 | 36.5 | 2.8 | 5.9 | 47.2 |
| 8.3 | 30.5 | 1.5 | 13.5 | 46.3 |
| 6.0 | 36.4 | 3.2 | 6.3 | 48.1 |
| 9.8 | 37.3 | 1.9 | 6.9 | 44.0 |
| 7.6 | 34.1 | 2.0 | 7.8 | 48.5 |
| 9.3 | 34.8 | 1.5 | 6.9 | 47.4 |
| 5.9 | 29.9 | 1.6 | 8.9 | 53.7 |
| 5.6 | 26.9 | 1.3 | 6.2 | 59.9 |
| 6.7 | 27.3 | 1.4 | 8.7 | 55.9 |
| 6.4 | 30.2 | 1.9 | 9.2 | 52.3 |
| 9.1 | 33.4 | 1.4 | 7.2 | 48.9 |
| 7.7 | 37.6 | 1.5 | 5.6 | 47.6 |
| 11.9 | 36.7 | 1.4 | 4.1 | 46.0 |
| 14.2 | 35.5 | 1.0 | 4.8 | 44.6 |
| 10.5 | 28.7 | 1.3 | 14.3 | 45.2 |

Average:

| | | | | |
|---|---|---|---|---|
| 8.53 | 34.00 | 1.94 | 7.46 | 48.10 |

Note: Data represents the EDX analysis (TEM 200kV) of twenty randomly chosen inclusions.

Table 3-7 JB34 Inclusion Chemical Analysis

| Sample ID | Acicular Ferrite [%] | Standard Deviation [%] |
|---|---|---|
| MV14 | 14.79 | 1.62 |
| JB32 | 8.33 | 1.26 |
| JB33 | 8.13 | 1.25 |
| JB34 | 5.00 | 0.994 |

Table 3-8 Weld Metal Acicular Ferrite Percentages

| Test # | MV14 [HV] | JB32 [HV] | JB33 [HV] | JB34 [HV] |
|---|---|---|---|---|
| 1 | 316.8 | 267.2 | 257.8 | 244.1 |
| 2 | 322.7 | 256.0 | 259.7 | 258.4 |
| 3 | 333.2 | 258.1 | 259.4 | 236.2 |
| 4 | 317.6 | 271.1 | 251.6 | 230.9 |
| 5 | 320.2 | 263.1 | 234.9 | 240.0 |
| 6 | 316.8 | 266.6 | 273.7 | 249.8 |
| 7 | 297.1 | 260.9 | 258.7 | 240.8 |
| 8 | 290.8 | 269.8 | 251.3 | 244.4 |
| 9 | 326.6 | 265.6 | 235.9 | 262.4 |
| 10 | 323.6 | 270.8 | 237.5 | 255.7 |
| **Average:** | 316.54 | 264.92 | 252.05 | 246.27 |

Table 3-9 Hardness Data

| Sample I. D. | HV [Vickers] | $H_B$ [Brinell] | $S_U$ [kpsi] (MPa) | $S_Y$ [kpsi] (MPa) |
|---|---|---|---|---|
| **MV14** | 316.54 | 299.25 | 134.66 (927.68) | 121.19 (834.91) |
| **JB32** | 264.92 | 251.92 | 113.36 (780.95) | 102.02 (702.86) |
| **JB33** | 252.05 | 241.05 | 108.47 (747.26) | 97.62 (672.53) |
| **JB34** | 246.27 | 234.92 | 105.71 (728.25) | 95.14 (655.43) |

Table 3-10 Tensile / Yield Strength Data

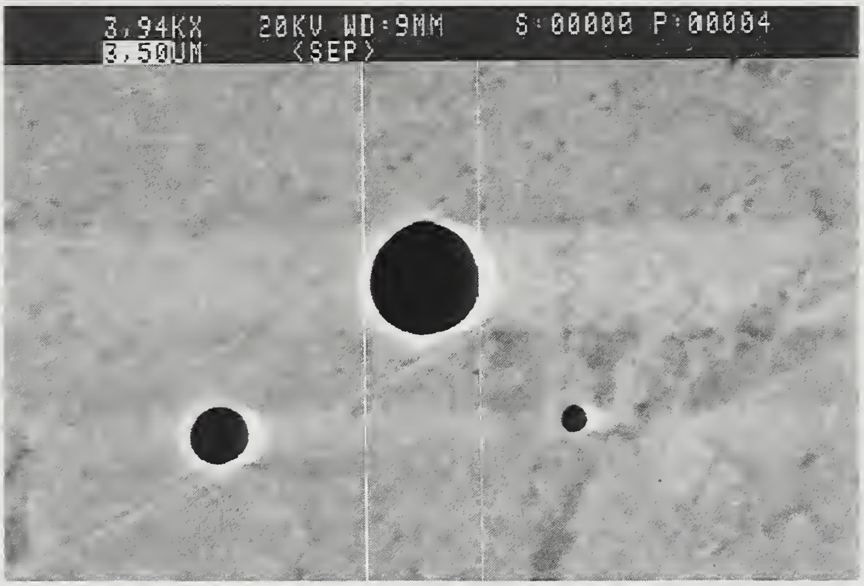
3,94KX 20KV WD:9MM S:00000 P:00004
3,50UM <SEP>

Figure 3-1 Typical Inclusion Field and Method of Diameter Measurement

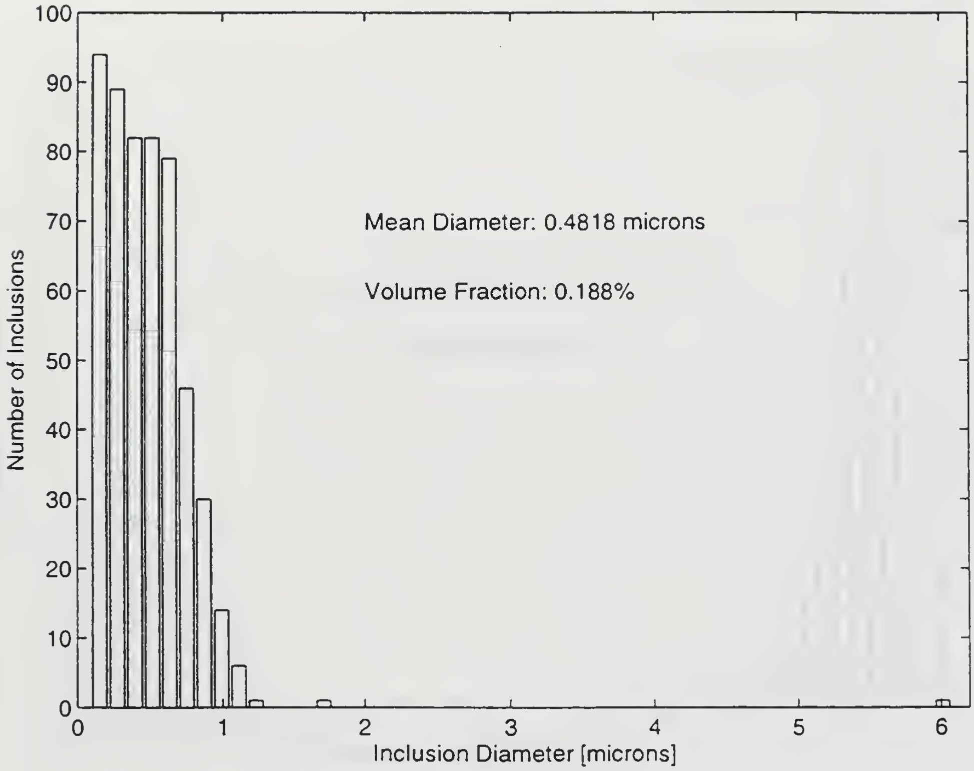

Figure 3-2. MV14 Inclusion Distribution

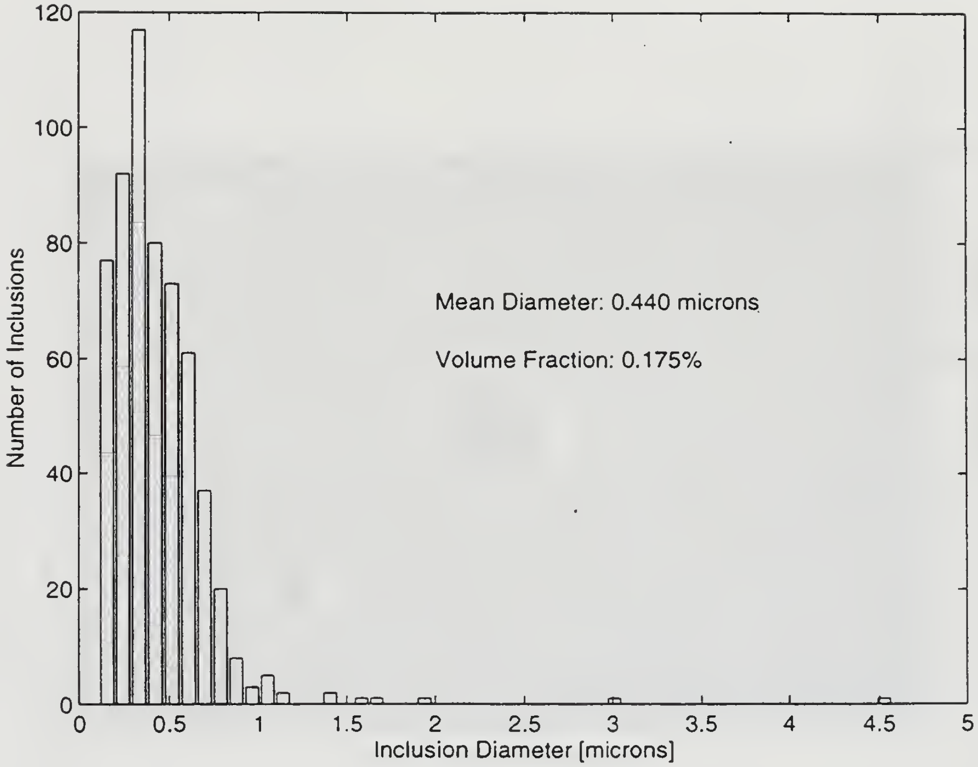

Figure 3-3. JB32 Inclusion Distribution

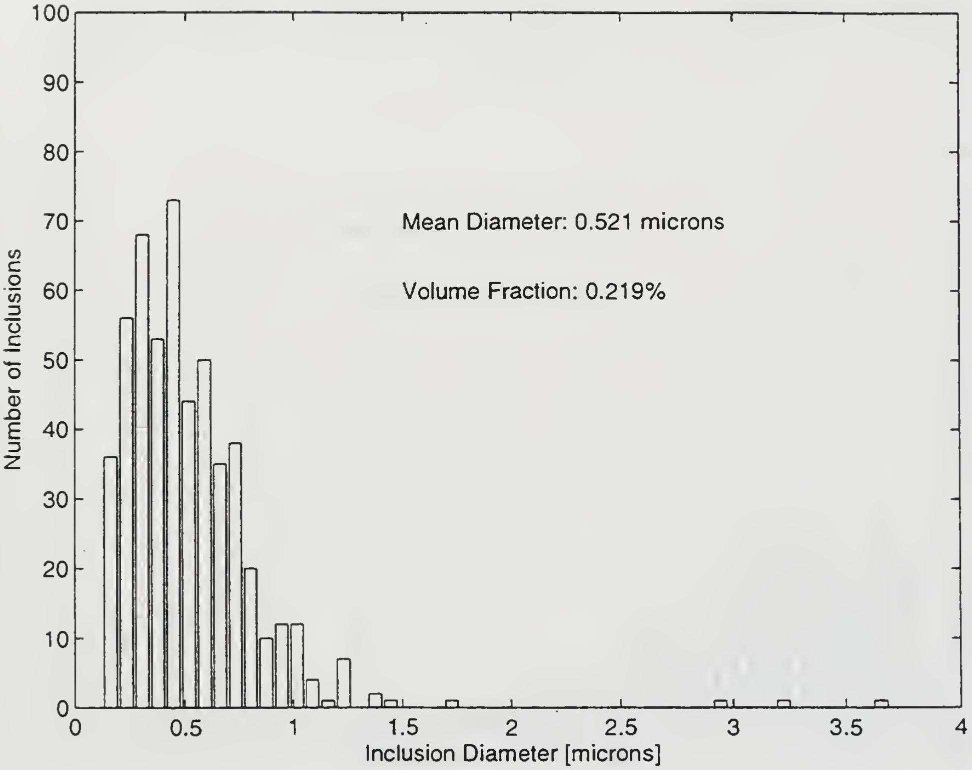

Figure 3-4 JB33 Inclusion Distribution

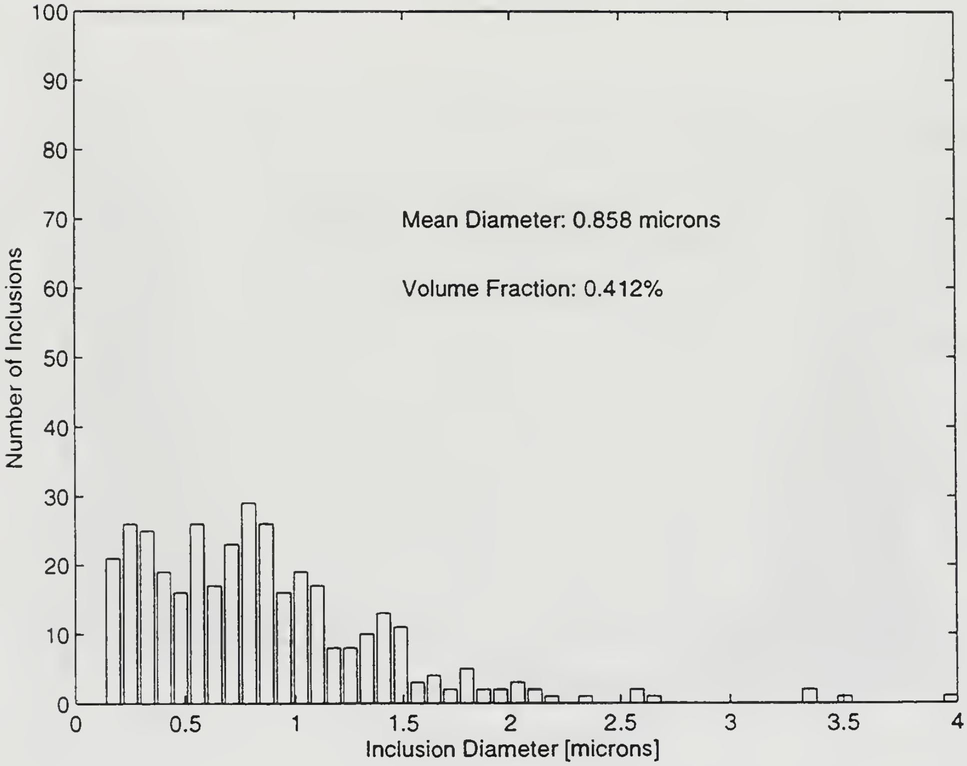

Figure 3-5. JB34 Inclusion Distribution

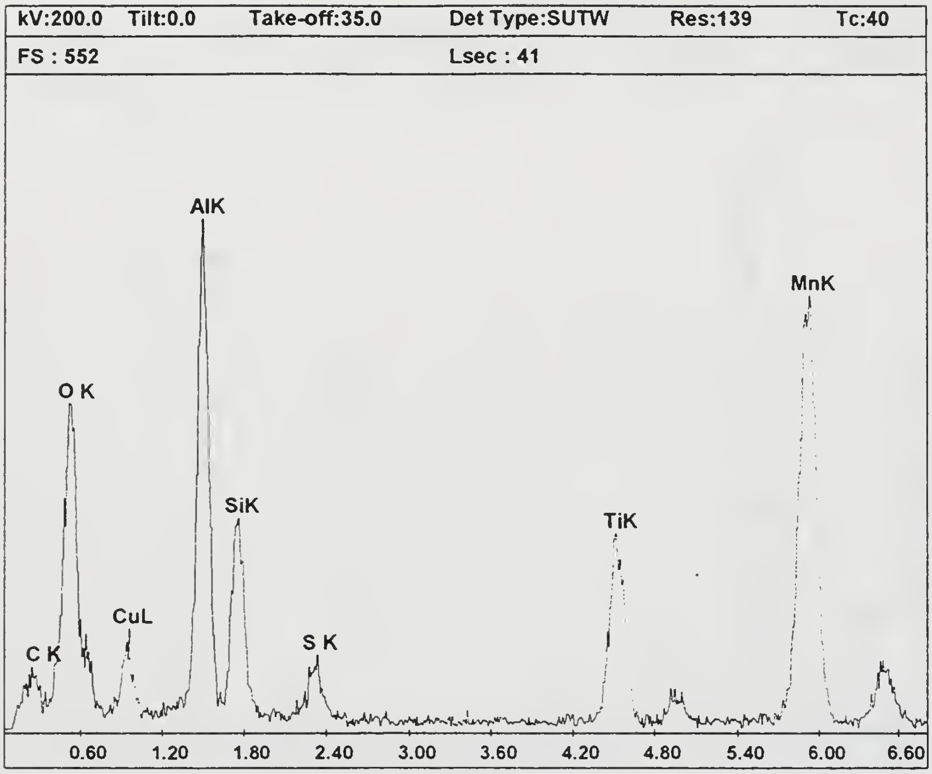

Figure 3-6. Typical TEM EDX Spectrum MV14

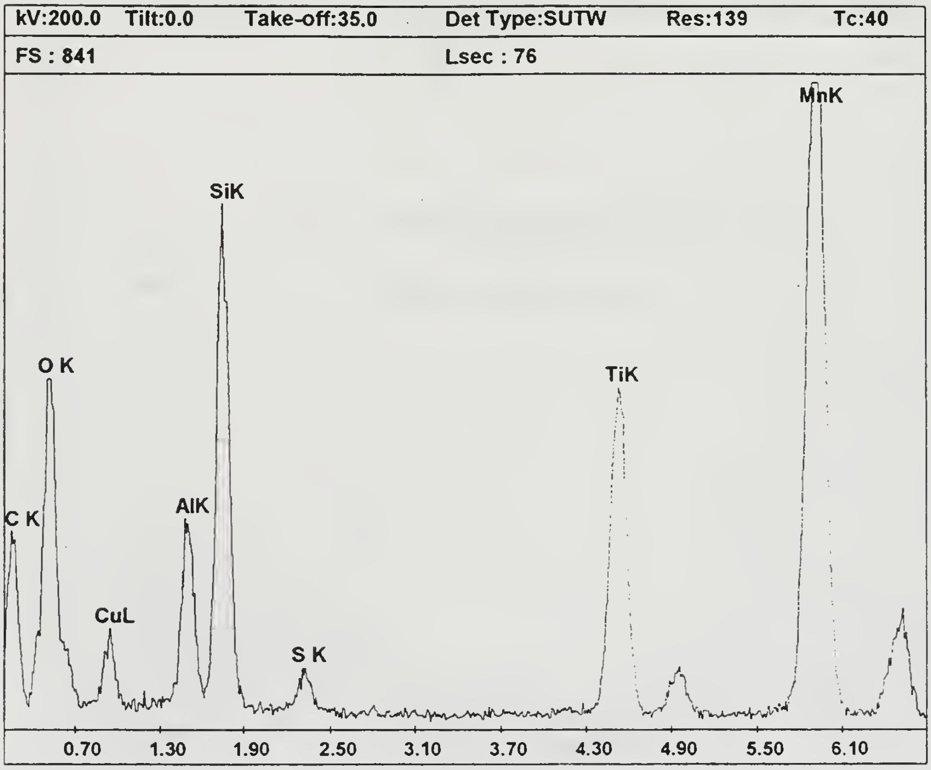

Figure 3-7 Typical TEM EDX Spectrum JB32

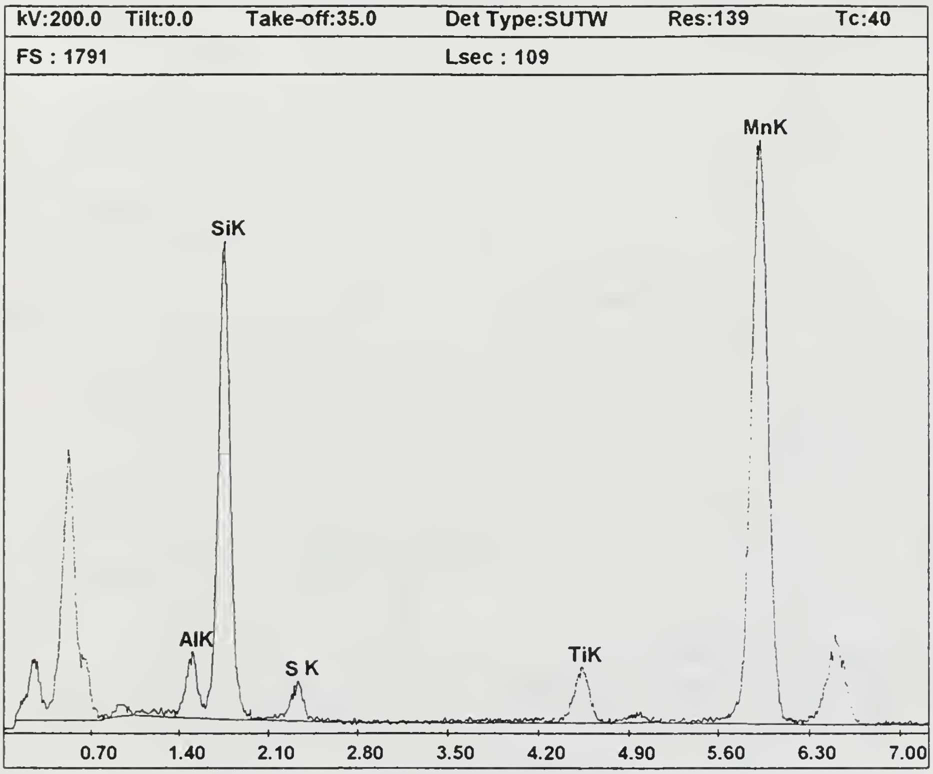

Figure 3-8 Typical TEM EDX Spectrum JB33

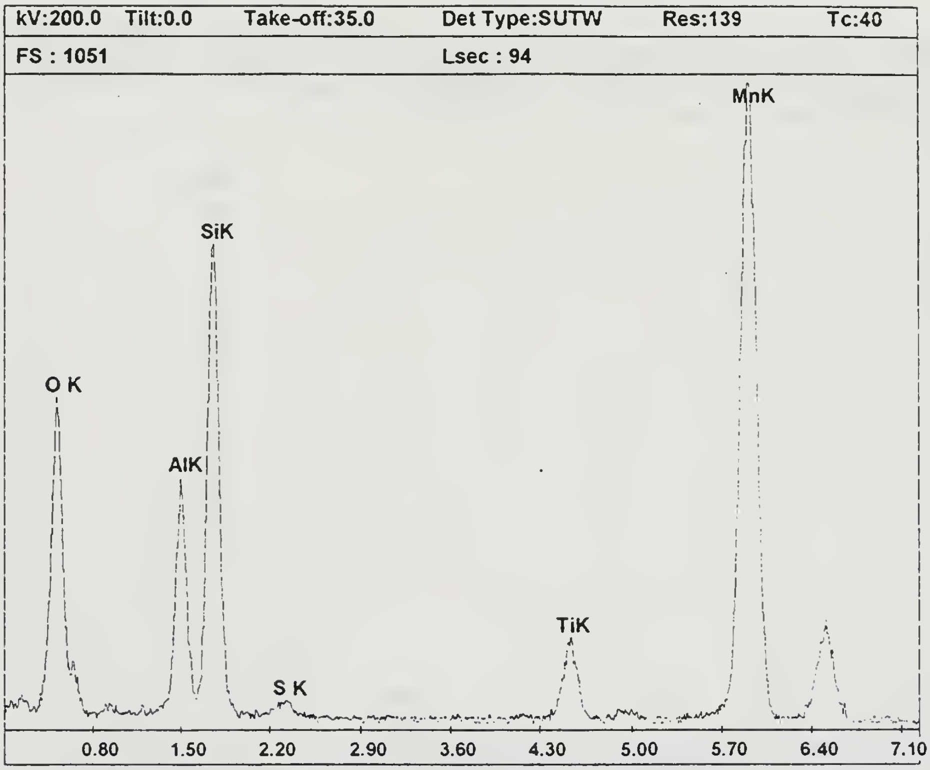

Figure 3-9 Typical TEM EDX Spectrum JB34

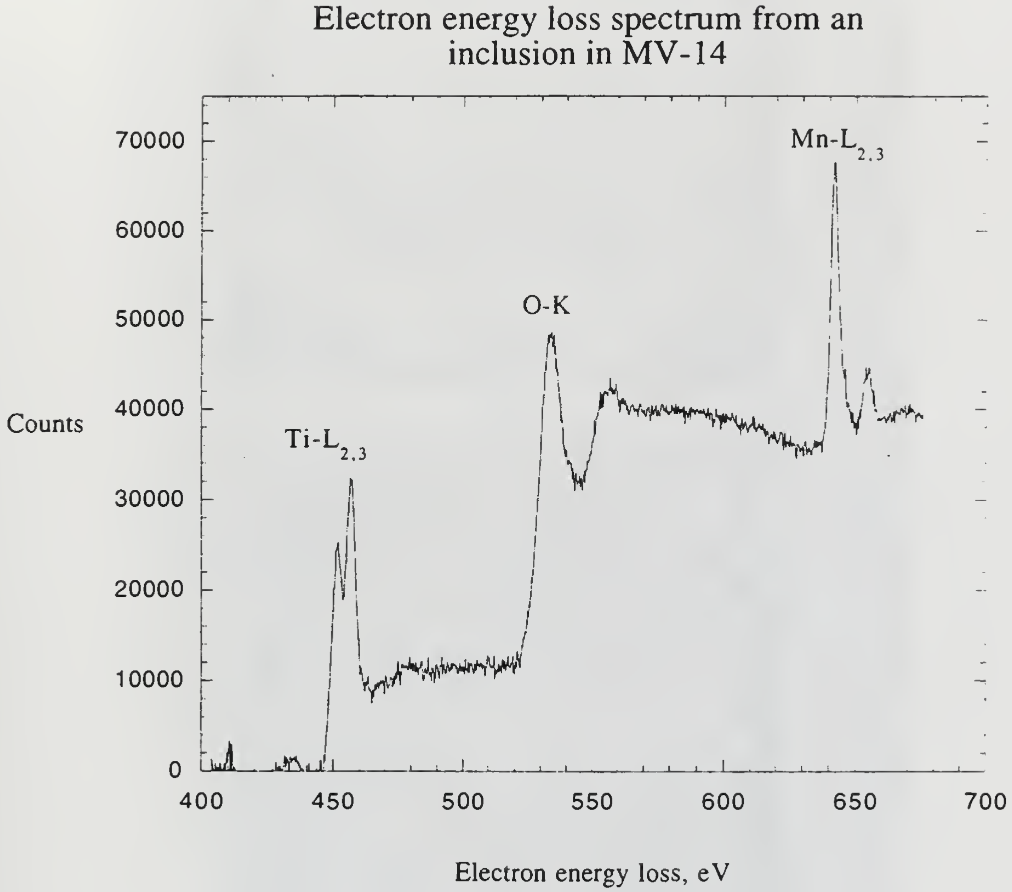

Figure 3-10 Typical PEELS Spectrum MV14

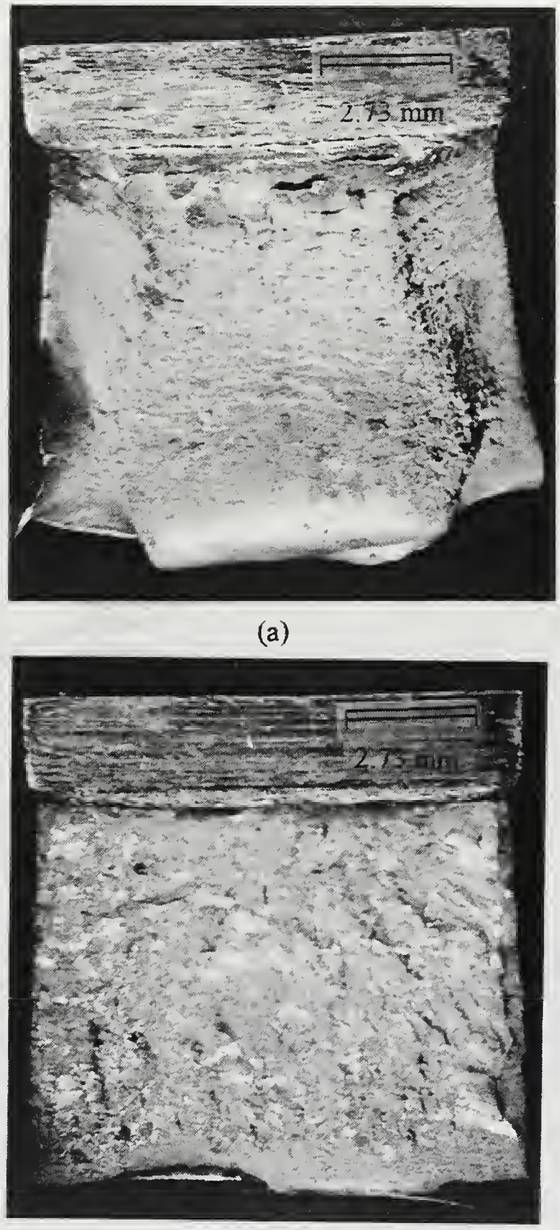
2.73 mm
2.73 mm

(a)

(b)

Figure 3-11 (a) Upper Shelf, and (b) Lower Shelf CVN Fracture Surface MV14

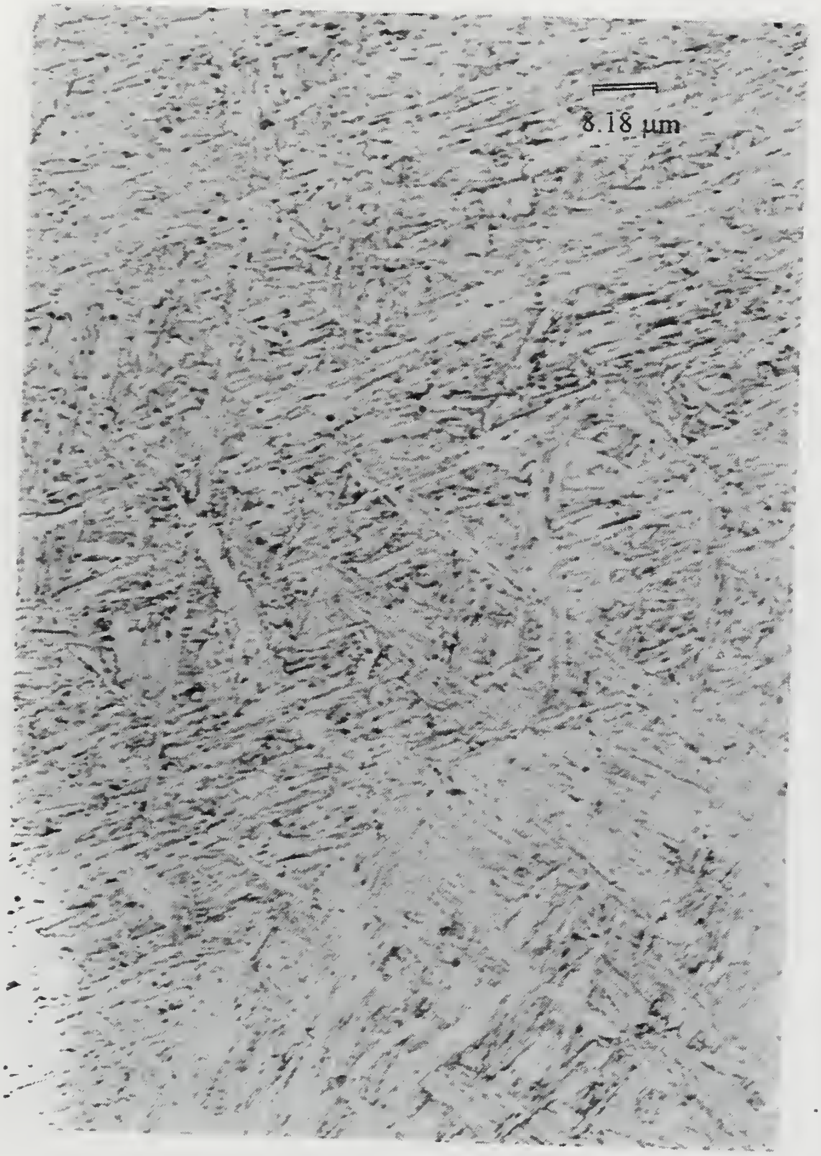

Figure 3-12 Representative Fusion Zone Microstructure MV14

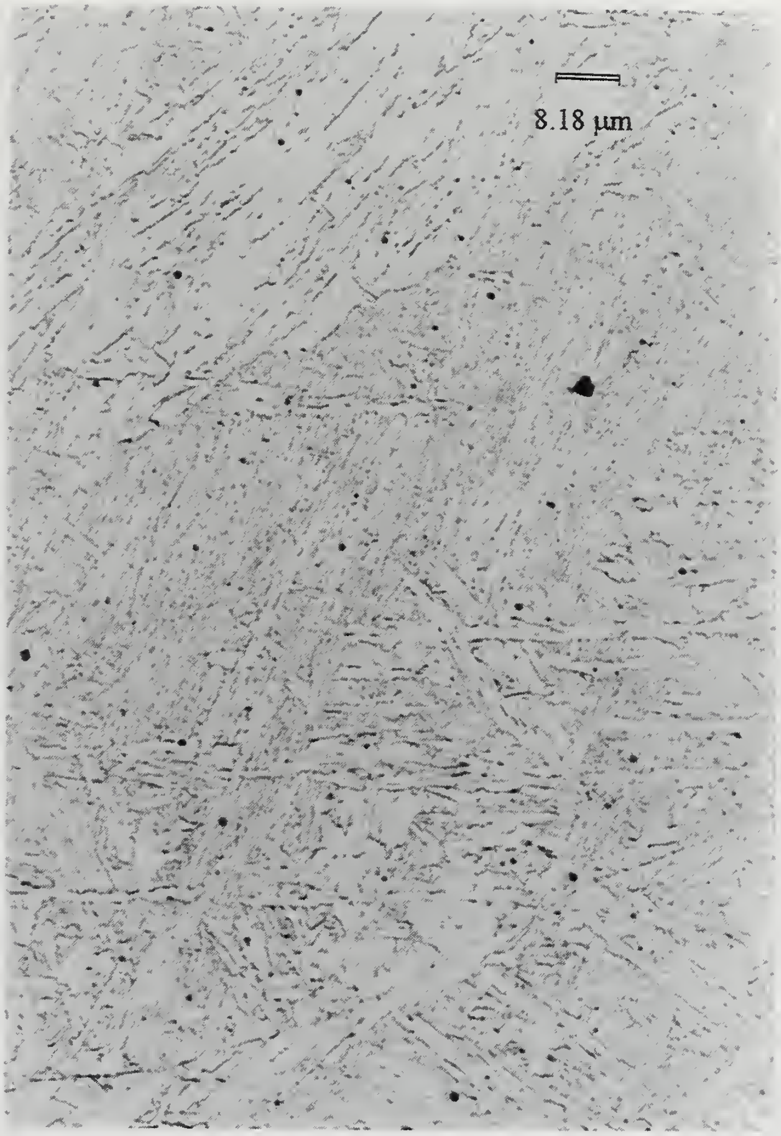

Figure 3-13 Representative Fusion Zone Microstructure JB32

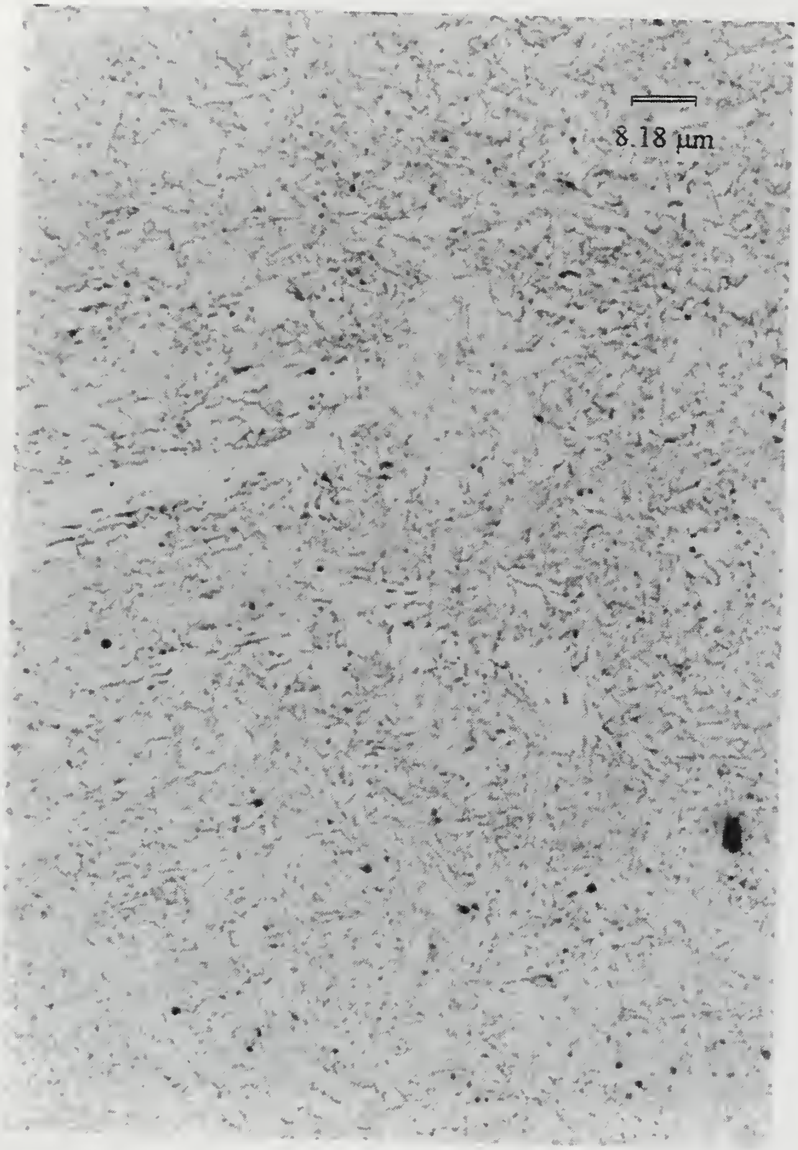

Figure 3-14 Representative Fusion Zone Microstructure JB33

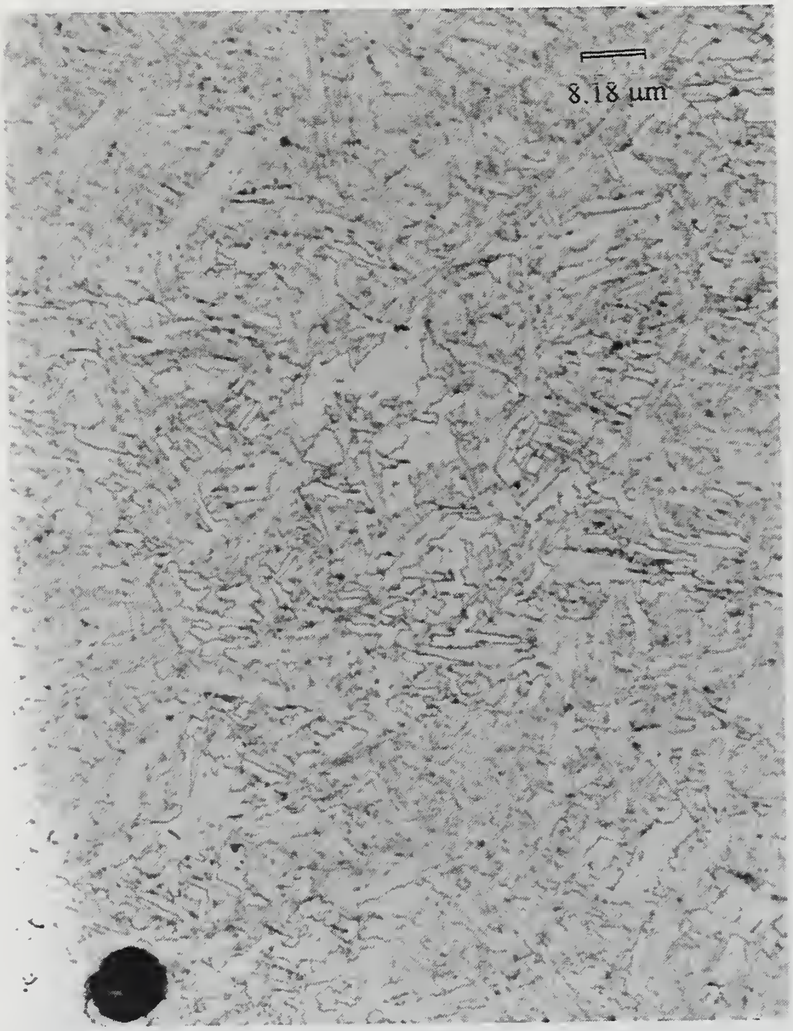

Figure 3-15 Representative Fusion Zone Microstructure JB34

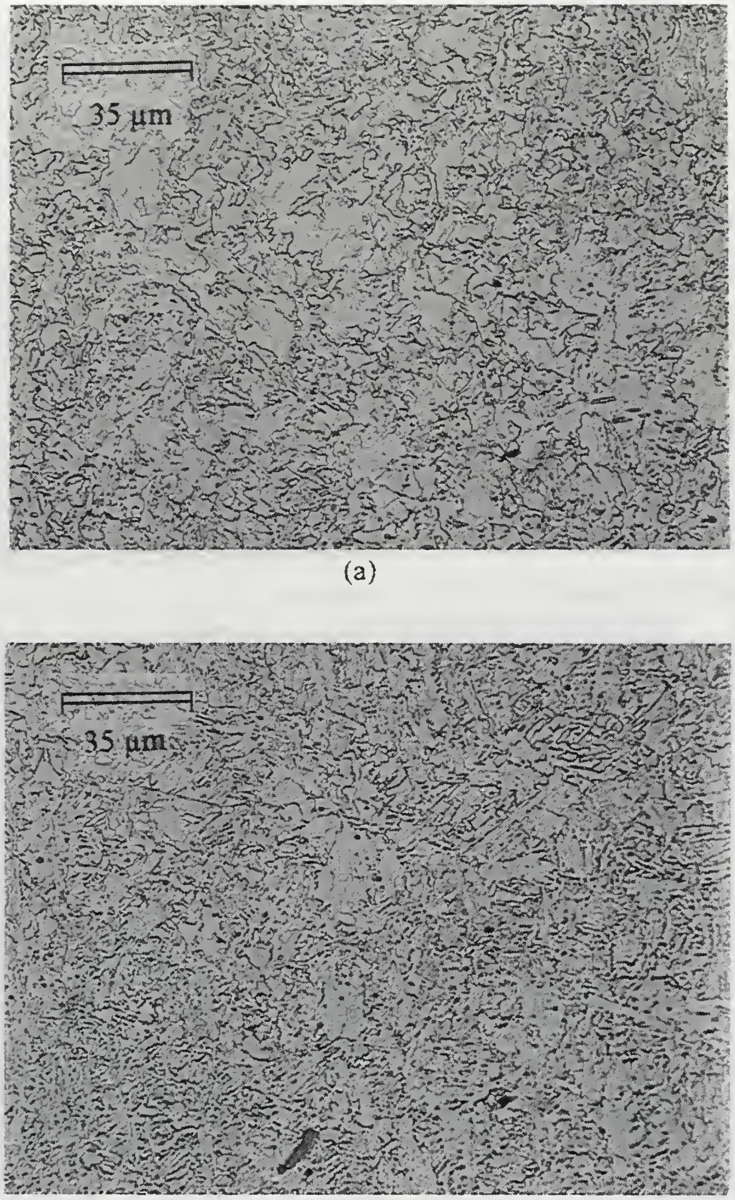

(a)

(b)

Figure 3-16 Typical Fusion Zone Micrographs at 500X used for Acicular Ferrite Percentage Calculations (a) JB33, (b) JB34

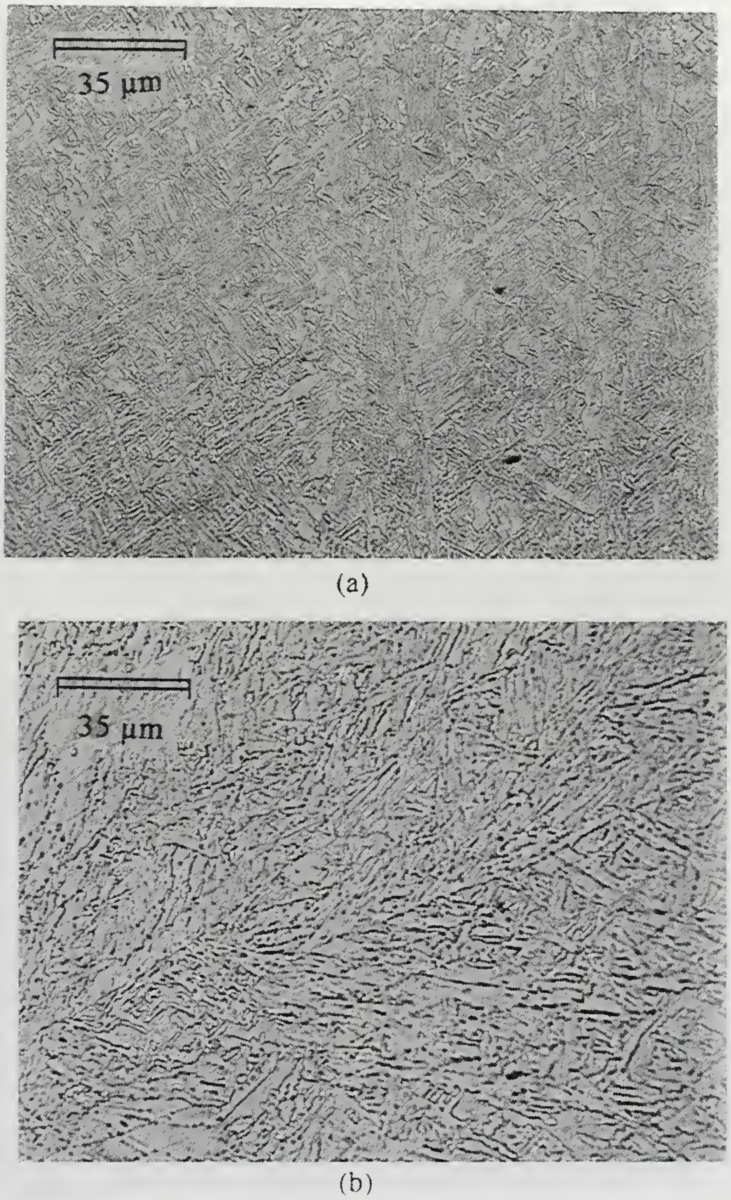

Figure 3-17 Typical Fusion Zone Micrographs at 500X used for Acicular Ferrite Percentage Calculations (a) MV14, (b) JB32

# IV. ANALYSIS, RESULTS, AND DISCUSSION

## A. WELD METAL CHEMISTRY

The final weld metal composition, shown in Table 4-1, is dependent on the compositions of the base plate, the filler wire, and the cover gas. The filler wire composition for both oxygen and nitrogen are very low for typical GMAW applications due to the method of fabrication (vacuum degassing). The nitrogen levels of the resulting weld metal remain low for typical GMAW welds and indicate an effective cover gas in shielding the weld pool from atmospheric contamination. While weld metal nitrogen levels remain low, the weld metal oxygen levels increase. Increased cover gas oxygen leads to increased weld metal oxygen content and increased 'consumption' of the deoxidizing elements Mn, Al, Ti, Si and Zr (if present). Figure 4-1 illustrates the linear increase of weld metal oxygen content with cover gas oxygen content. In the development of Figure 4-1, 100% of the oxygen in the cover gas was assumed to be available for reaction in the weld pool for welds with Ar-$O_2$ cover gas combinations (JB32, JB33, JB34).[Ref.19,28] For the weld with an Ar-$CO_2$ (C5) cover gas (MV14), the disassociation of $CO_2$:

$$CO_2 \rightarrow CO + \frac{1}{2}O_2 \tag{4.1}$$

$$CO \leftrightarrow C + O \tag{4.2}$$

is anticipated to result in less than 100% of the oxygen being available for reaction in the weld pool.[Ref.19,28] Equation 4.3 was utilized to calculate the effective oxygen content (in volume %) of the shielding gas when using carbon dioxide:

$$EffO_2 = -0.088 + 0.148[CO_2]^{1.524} \tag{4.3}$$

where,

$EffO_2$ = Effective Oxygen Content [vol.%]
$CO_2$ = volume percent of carbon dioxide in cover gas.[Ref.28]

The increased oxygen content of the weld pool results in the depletion of the strong deoxidizing elements as non-metallic inclusions are formed. Referring to Table 4-1, the chemical composition of the filler wire is compared to the final weld metal chemical composition for welds JB32, JB33, and JB34. MV14 is plotted for comparison only due to the use of C5 cover gas for this weld and a slightly higher heat input (62 instead of 60 KJ/in). The composition of the strongest deoxidizer, aluminum (Al), remains constant as the oxygen content increases. While it is anticipated that the Al content would decrease as the oxygen level increases, the low levels of Al within the filler wire, and weld metal, are very near the level of precision reported in Table 3-3 for measuring the Al content.( 0.003 wt.% in the weld metal compared to a level of precision of 0.002 wt %) These low levels of Al are believed to be too low for trend identification purposes. The Titanium (Ti) levels for the weld metal of JB32, JB33, and JB34 also appear to remain fairly constant as the oxygen level increases. The level of Ti in the weld metal is also anticipated to decrease as the oxygen level increases; however, the Ti levels of the weld metal indicate a significant reduction in the filler wire Ti levels, indicating a possible maximum has been reached in reactivity. The manganese (Mn), nickel (Ni), and silicon (Si) contents are also seen to decrease with increasing oxygen contents in welds JB32, JB33, and JB34 indicating the anticipated increased involvement of these alloys in the deoxidation of the weld pool and the resulting formation of non-metallic inclusions. The molydemum (Mo) content of these welds is seen to decrease with increasing oxygen activity as well, with the exception of JB32, which shows a level greater than the filler wire, or the base plate, composition. The Mo level reported for the weld metal of JB32 is believed to be in error and will be estimated at 0.5 weight percent for further calculations..

The carbon content of the weld metal is seen to decrease with increasing oxygen content due to the formation of carbon dioxide gas and the resulting escape to the atmosphere.(Eqn. 4.2) MV14 is seen to have the highest carbon content due to the disassociation of the C5 cover gas into carbon and oxygen and the resulting entrapment of carbon in the weld pool.(Eqn. 4.1) Carbon has the strongest effect of all alloying elements on the hardenability of steel. The weld metal final hardness (strength) is determined primarily by the depletion of the final carbon content of the weld metal , and to a lesser extent the weak depletion of the inclusion forming alloys (Mn, Si, Al, and Ti). As illustrated in Equation 4.4, the hardness of steel alloys are often expressed in terms of the carbon equivalent (CE) for comparison purposes.[Ref. 22]

$$CE = C + \frac{Mn + Si}{6} + \frac{Ni + Cu}{15} + \frac{Cr + Mo + V}{5} \tag{4.4}$$

In this equation, carbon has a one to one effect on strength (CE) while, other alloys have a reduced impact due to the constants in their denominators. Figure 4-2 demonstrates the decrease in the weld metal carbon equivalent as the cover gas oxygen content increases. The overall effect of the decrease in the weld carbon equivalent is confirmed by Figure 4-3; where the weld metal hardness vs. weld metal oxygen content is plotted. Increasing cover gas oxygen results in decreasing hardness. MV14 has the highest hardness due to its high carbon content, and was not included in the trend due to the additional contribution of the C5 cover gas.

## B. NON-METALLIC INCLUSIONS

### 1. Size and Volume Fraction

The inclusions contained within the fusion zone of all welds were analyzed for mean diameter and volume fraction data as described in section IIIC. Figures 4-4, and 4-5 graphically illustrate the mean inclusion diameter vs. weld metal oxygen content, and the inclusion volume fraction vs. weld metal oxygen content respectively. With weld MV14 once again treated as an outlier for studying trends, the data associated with welds JB32, JB33, and JB34, illustrate that with increasing weld metal oxygen content the mean inclusion size and volume fraction both show a strong increase which appears to be linear. The increase in inclusion mean diameter and volume fraction with weld metal oxygen content is anticipated since increased oxygen content results in the increased reaction of deoxidizing elements within the weld pool leading to more numerous and large inclusions.

### 2. Inclusion Chemical Composition

Weld metal non-metallic inclusions, captured by carbon extraction and analyzed in the TEM by EDX, were found to be predominantly spherical in shape, multi-phase, and composed of the following elements combined with oxygen, sulfur, or a combination of both: Al, Ti, Si, and Mn. In addition to these elements copper and carbon were identified by EDX spectra analysis of inclusions. The copper signal arose primarily from the copper grids on which the samples were mounted, although occasionally CuS was found in the inclusions. The carbon spectra indications were believed to be from the film from the carbon extraction technique. Typical spectra from each samples inclusions are illustrated in Figures 3-6 through 3-9.

Figure 4-6 illustrates the variation in inclusion aluminum content vs. weld metal oxygen content. Although MV14 was produced with a different type of cover gas (which means the cover gas oxygen activity was lower) there is evidence that the Al content of the inclusions is decreasing with increasing weld metal oxygen content. It should be noted however that for the three welds made with $Ar/O_2$ combinations a downward trend (if any) is not clear. This is because the Al content of the weld is low and close to the equilibrium value.

Figure 4-7 illustrates the variation in inclusion titanium content vs. weld metal oxygen content. Significant data scatter was noted for all welds, as well as a weak decreasing trend in inclusion titanium content for welds JB32, JB33, and JB34. Titanium, as a strong de-oxidizer, is expected to decrease with increasing weld metal oxygen content.

Figure 4-8 illustrates the variation in inclusion silicon content vs. weld metal oxygen content. It was difficult to detect a trend for silicon. With the most reactive elements Al, and Ti, reacting with the available oxygen at low oxygen levels and becoming depleted, it is anticipated that the more abundant silicon would then react with the excess oxygen at higher levels. This silicon reaction at higher oxygen levels should result in increasing inclusion silicon levels with increasing weld metal oxygen content.

Figure 4-9 illustrates the variation in inclusion manganese content vs. weld metal oxygen content. A weak increasing trend of inclusion manganese content was noted with increasing weld metal oxygen. As with silicon, this increasing trend in inclusion manganese content is anticipated. At higher oxygen levels with the strong de-oxidizers depleted, silicon and manganese should become a larger contributor to inclusion composition.

In addition to EDX analysis of twenty randomly chosen inclusions, several thin inclusions were identified for PEELS analysis, as well as EDX analysis of specific phase areas identified within the inclusions. Figure 4-9 illustrates a typical thin inclusion with two phases (one dark and faceted and the other lighter and spherical), with the EDX spectra from each phase. EDX analysis of each phase was accomplished by utilizing a small probe size and hitting only the area of interest. As noted in Figure 4-10, the dark and faceted area was found to rich in titanium and manganese, while the lighter spherical area was found to be rich in silicon and manganese. Several thin inclusions from various weld samples were probed and found to be similar to Figure 4-9. In all cases, faceted areas of the inclusions were found to be rich in titanium as compared to the other phases of the inclusion. PEELS and diffraction, analysis of several thin inclusions was also conducted, with results indicating the titanium present to be in the form of TiO, rather than $TiO_2$ or $Ti_2O_3$. While PEELS spectra were readily obtained, the PEELS mapping of different compounds/elements proved to be difficult because the thin inclusions and carbon films were damaged by the excessive amount of time/energy required for probing and mapping inclusions.

## C. MECHANICAL PROPERTIES

The objective of the current US Navy welding consumable research is to develop a solid filler wire for use with GMAW that meets the requirements of MIL-120S. MIL-120S requires the following properties for the GMAW welds:

- yield strength between 703 MPa (102 ksi), and 848 MPa (123 ksi), and
- Charpy V-notch minimum toughness of 61 J (45 ft-lb.) at -51°C (-60°F) and 81 J (60 ft- lb.) at -18°C (0°F).[Ref. 3]

### 1. Yield Strength

Figure 4-11 illustrates the weld metal yield strength vs. weld metal oxygen content. With MV14 plotted for comparison purposes only, JB32 ,JB33, and JB34, illustrate that yield strength decreases linearly with increasing oxygen content. In comparison with the requirements of MIL-120S, MV14 and JB32 meet yield strength requirements while JB33 and JB34 do not. Yield strength is primarily a function of hardness and as illustrated in Figure 4-3, the hardness of the welds decrease with increasing oxygen content. The increased oxygen content depletes the carbon and the de-oxidizing alloys by forming carbon monoxide gas and non-metallic inclusions respectively. With carbon as the most effective hardening alloy, Figure 4-12 illustrates the weld metal hardness vs. weld metal carbon content. With JB32 ,JB33, and JB34 utilized for trends ,and MV14 plotted only for comparison, the increasing weld metal carbon content results in a linear increase in weld metal hardness as anticipated.

### 2. Impact Properties

NSWC reported data for Charpy V-notch tests and Fracture Appearance Transition Temperatures (FATT) are illustrated in Figures 4-13 through 4-16. Welds MV14, JB32, and JB33 meet MIL-120S requirements while JB34 does not meet specifications. Figure 4-17 illustrates FATT vs. weld metal oxygen content. FATT temperatures for welds JB32 ,JB33, and JB34, show a weak linear increase with increasing oxygen content - indicating a loss of toughness. While the FATT temperature for MV14 is reported to be significantly better than JB32 (-89 vs.-70°C), the data scatter in the Charpy tests for MV14 (Fig. 4-13) suggests that the true value of MV14 FATT may be closer to the value reported for JB32. Figure 4-18 illustrates the weld metal hardness vs. FATT data for all welds. For JB32 ,JB33, and JB34, increasing hardness results in a lower FATT temperature, with MV14 being the hardest weld and also the weld with the lowest FATT temperature. This increase in strength and toughness is a very important trend and indicates the importance of the size and volume fraction of inclusions on weld metal toughness. The smaller the mean inclusion size, and a lower volume fraction of inclusions, results in a stronger and tougher weld. MV14 and JB32 have the highest Mn and carbon contents, smallest inclusion mean diameter and volume fraction, and result in the strongest and toughest welds. MV14 and JB32 both meet MIL-120S requirements for strength and toughness. Increased size and volume fraction of inclusions provides increased nucleation sites for micro-void formation during failure, and increased crack propagation paths.

As mentioned in section IV(A) the filler wire and resulting weld metal nitrogen levels are low for typical GMAW weldments. These low nitrogen levels may be a contributing factor to the overall toughness of the weld and should be investigated in future research.

## D. FRACTOGRAPHY

Figure 3-11 illustrates the macrographic upper and lower shelf fracture surfaces for sample MV14. These samples are particularly interesting in that the lower shelf fracture surface ($-100^0$ C) still demonstrates some ductile features at the outermost edge of the fracture surface. Figure 4-19 illustrates the microscopic (SEM photo) upper and lower shelf fracture surfaces for sample MV14. The upper shelf , or high temperature, fracture surface illustrates a typical ductile fracture surface: A dimpled and topographical appearance with a large number of micro-voids visible. The lower shelf fracture surface failure mode appears to be primarily brittle cleavage with some ductile features (micro-voids). Of particular interest is the inclusion (denoted by the arrow) centered within a micro-void, indicating the initiation site for the ductile mode of failure.

## E. MICROSTRUCTURAL AND MACROSTRUCTURAL ANALYSIS

### 1. Macroscopic

Figure 4-20 illustrates a macrograph of the GMAW weld at approximately 3x. Readily discernible in the montage of photographs (looking from outer edge of weld toward the center) is the base metal, heat affected zone (both fine and coarse grained), and the papullary nature (upright horseshoe) of the individual GMAW weld passes. The grain structure of the individual passes is seen to be columnar in appearance and growing toward the center of the weld, or high temperature regions.

### 2. Microscopic

Figure 4-21 illustrates a TEM bright field photograph of the typical microstructure seen for all welds. While some acicular ferrite, retained austenite and lath martensite, were visible, the microstructure of all welds was primarily granular ferrite. This microstructure was anticipated due to the calculated cooling rate through the critical temperature range (800-500$^0$ C) of 7.5 to 10 seconds (Eqn. 2.3), and the combination of the final weld metal alloy content and oxygen level. Figure 4-22 illustrates the effects of heat input, cooling rate, alloy content, and oxygen content on weld metal microstructure. Optical photography observations confirm TEM observations.

Optical photographs Figures 3-16 and 3-17 were used to calculate acicular ferrite percentages. Figure 4-23 illustrates a plot of acicular ferrite vs. weld metal oxygen content. Using weld JB32, JB33, and JB34 for trending purposes, the acicular ferrite percentage was seen to decrease with increasing weld metal oxygen content. While this decreasing trend agrees with results predicted by Figure 4-22, the calculation of acicular ferrite percentages are highly dependent on the personal observations (expertise) of the author and may be subject to greater than statistical error. The low acicular ferrite percentages present in the welds studied were due primarily to the fast cooling rate (7.5-10 seconds), and the lack of the optimum weld metal oxygen contents.(too low for welds MV14: 170ppm and JB32: 220ppm, and too high for JB34: 470ppm). Optimum conditions for acicular ferrite formation are 15seconds through the critical temperature range (800-500$^0$ C) and a weld metal oxygen content of 250ppm.[Ref. 22] JB33 has very nearly the optimum oxygen content at 260ppm, but the cooling rate remains less than optimum and appears to dominate in the final microstructural determinations.

# V. SUMMARY

## A. CONCLUSIONS

The weld metal strength and toughness requirements of MIL-120S were met by two of the welds in this study (MV14 and JB32). High strength and toughness were seen to be a function of:

- weld metal microstructure- determined primarily by the cooling rate from 800-500$^0$ C (a function of heat input), and
- low weld metal oxygen content (< 250ppm) which results in smaller mean inclusion size and volume fraction, and lower filler wire alloy dilution- primarily carbon.

The microstructure formed in the welds of all samples was primarily granular ferrite with some acicular ferrite. While acicular ferrite is thought to lead to optimum impact properties, the low percentages of acicular ferrite in all welds studied indicates that for an ultra low carbon steel filler wire used in the GMAW process, predominantly granular ferritic microstructures can achieve the required strength and toughness.(MIL-120S)

The increasing oxygen content of the cover gas and resulting weld metal, led to a reduction of the weld metal alloy constituents (used for strengthening in the place of carbon for HSLA-100 steel) due to the formation of non-metallic inclusions. These alloy constituents (Al, Ti, Mn, Si, S) formed multi-phase oxide/sulfide inclusions. Inclusion size and volume fraction were both found to increase with increasing weld metal oxygen content. EDX and PEELS analysis of selected thin inclusions from each weld sample revealed a segregation of phase areas. Phases which are high in titanium concentration typically have angular facets and are contained within the mostly spherical inclusion. The titanium compound present is believed to be TiO, although more work is needed to support this conclusion.

## B. RECOMMENDATIONS

The success of the experimental ultra low carbon filler wire in meeting MIL-120S requirements for strength and toughness should warrant further study. GMAW welds utilizing ultra low carbon filler wire should be studied with C5 cover gas at various heat inputs which may help in the formation of additional acicular ferrite. Also, GMAW welds with a fixed Ar-$O_2$ cover gas with oxygen levels below 250ppm should be studied at various heat inputs to judge the effects of cooling rate/heat input on strength and toughness properties. In order to determine the effect of the low nitrogen levels in the developmental filler wire on overall toughness, additional study should also be conducted to vary weld metal nitrogen levels.

| Element | HSLA-100 | Filler Wire | MV-14 | JB-32 | JB-33 | JB34 |
|---|---|---|---|---|---|---|
| C | 0.034 | 0.03 | 0.029 | 0.025 | 0.024 | 0.021 |
| Mn | 1.18 | 1.51 | 1.2 | 1.23 | 1.11 | 1.01 |
| Mo | 0.18 | 0.54 | 0.48 | 1.51 | 0.50 | 0.49 |
| Ni | 3.51 | 4.95 | 4.18 | 4.67 | 4.65 | 4.59 |
| Nb | 0.039 | < 0.002 | < 0.002 | 0.003 | 0.002 | 0.006 |
| Cr | 0.047 | 0.009 | 0.016 | 0.015 | 0.013 | 0.017 |
| Si | 0.25 | 0.35 | 0.28 | 0.26 | 0.18 | 0.19 |
| Cu | 1.25 | 0.003 | 0.18 | 0.16 | 0.19 | 0.3 |
| S | 0.002 | 0.002 | 0.005 | 0.002 | 0.002 | 0.003 |
| P | 0.008 | < 0.004 | 0.006 | < 0.004 | < 0.004 | < 0.004 |
| Al | 0.035 | 0.003 | 0.003 | 0.003 | 0.002 | 0.003 |
| Ti | 0.010 | 0.022 | 0.010 | 0.009 | 0.005 | 0.008 |
| N | 0.005 | 0.001 | 0.004 | 0.002 | 0.004 | 0.004 |
| O | 0.0009 | 0.0061 | 0.017 | 0.022 | 0.026 | 0.047 |
| V | 0.001 | 0.002 | 0.002 | 0.002 | 0.002 | 0.002 |
| H | 0.00009 | 0.00025 | 0.00013 | 0.00015 | 0.00018 | 0.00012 |
| B | < 0.005 | 0.0011 | 0.003 | 0.001 | 0.0008 | 0.0006 |

Note: All data in weight percent [wt. %].

Table 4-1 Chemical Composition of the Base Plate, Filler Wire, and Weld Metal

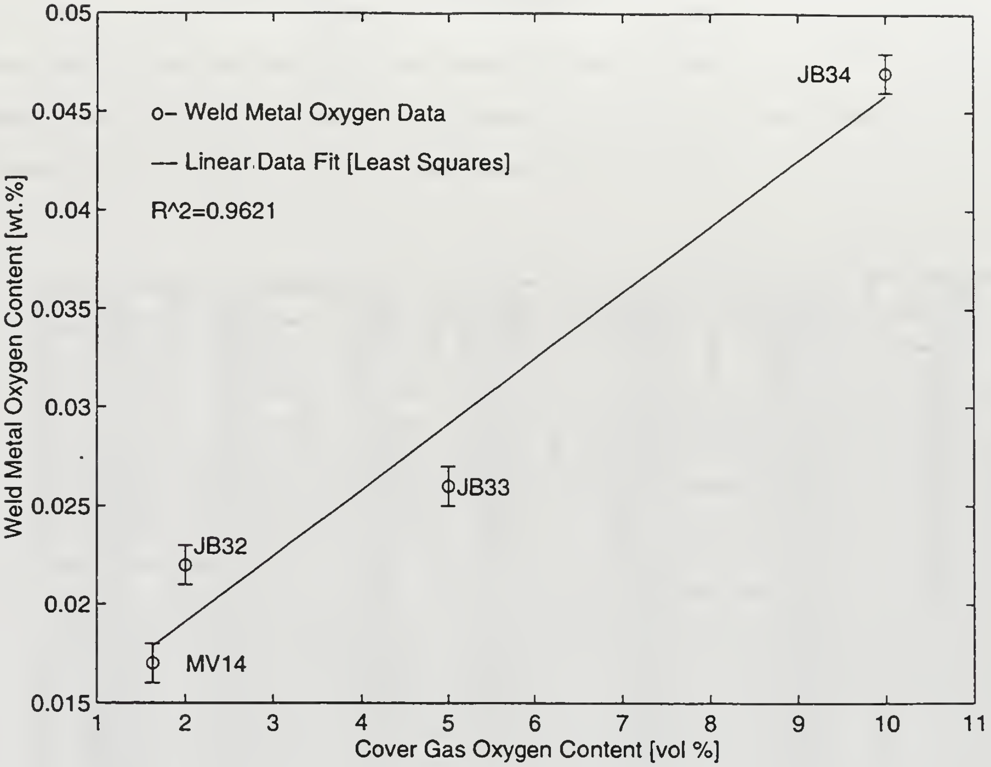

| Sample I.D. | Weld Metal Oxygen Content [wt%] | Cover Gas Oxygen Content [Vol.%] |
|---|---|---|
| MV14 | 0.017 | 1.63 |
| JB32 | 0.022 | 2.0 |
| JB33 | 0.026 | 5.0 |
| JB34 | 0.047 | 10.0 |

Figure 4-1 Weld Metal Oxygen Content vs. Cover Gas Oxygen Activity

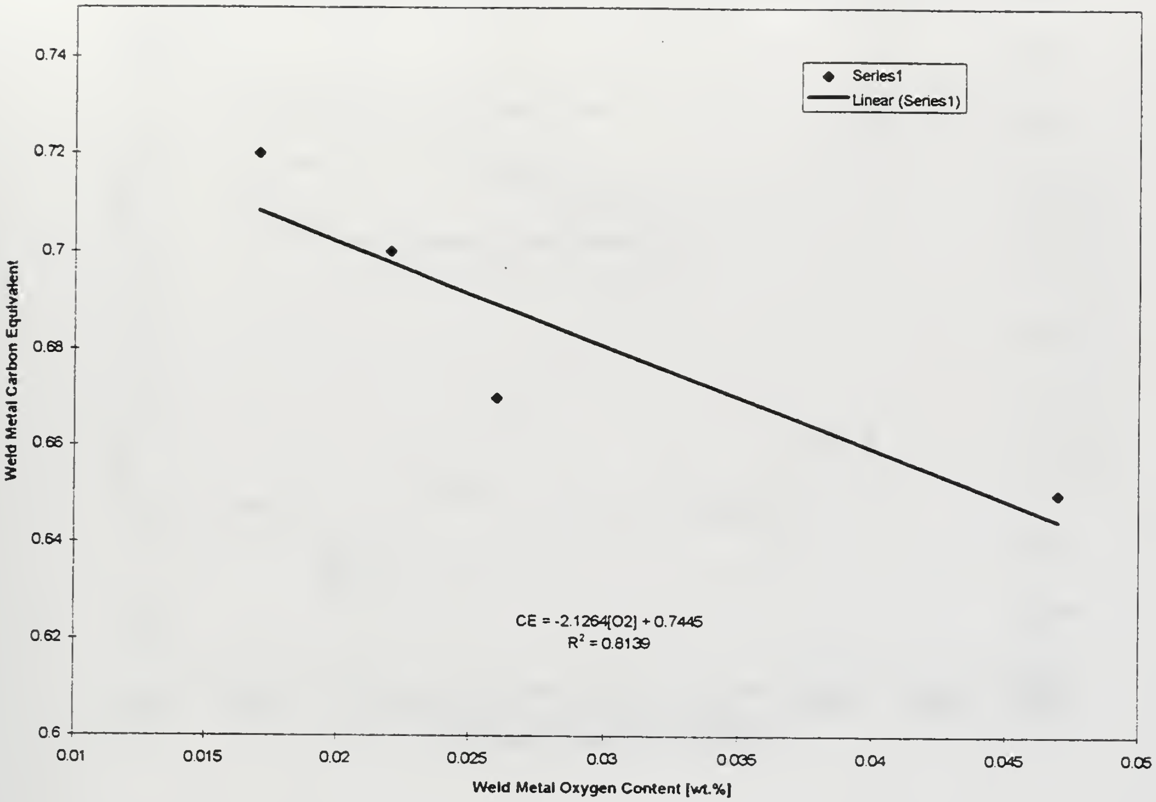

| Sample I.D. | Weld Metal Oxygen Content[wt%] | Carbon Equivalent |
|---|---|---|
| MV14 | 0.017 | 0.72 |
| JB32 | 0.022 | .070 |
| JB33 | 0.026 | 0.67 |
| JB34 | 0.047 | 0.65 |

Figure 4-2 Weld Metal Carbon Equivalent vs. Weld Metal Oxygen Content

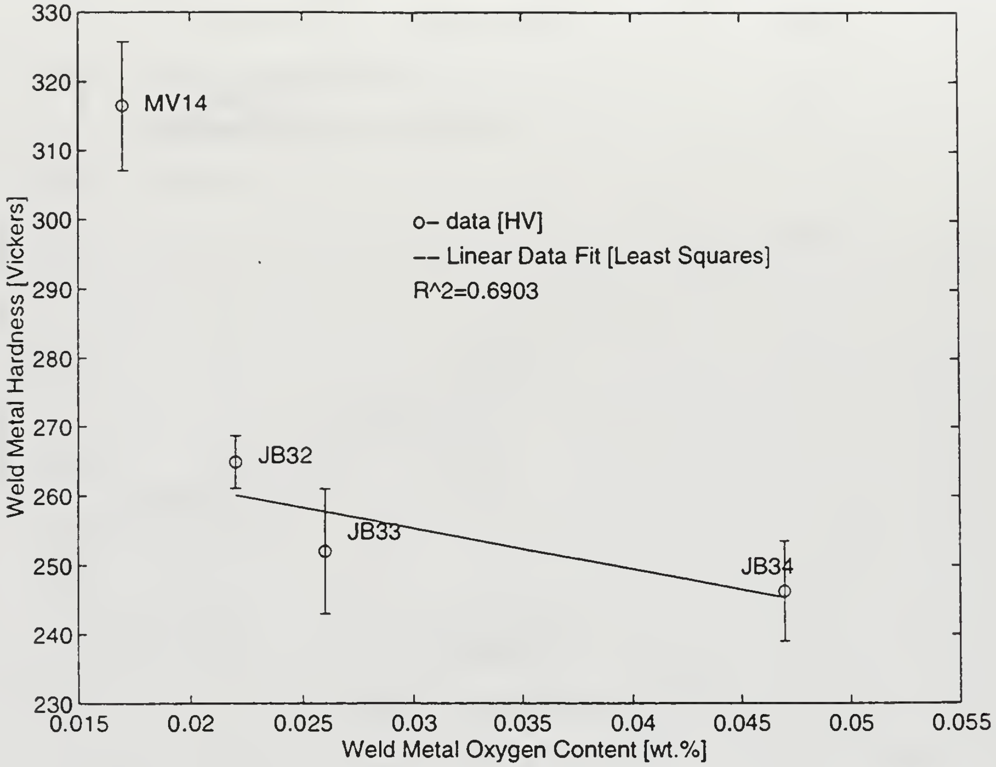

| Sample I.D. | Weld Metal Oxygen Content [wt%] | Hardness [Vickers] |
|---|---|---|
| MV14 | 0.017 | 316.54 |
| JB32 | 0.022 | 264.92 |
| JB33 | 0.026 | 252.05 |
| JB34 | 0.047 | 246.27 |

Figure 4-3 Weld Metal Hardness vs. Weld Metal Oxygen Content

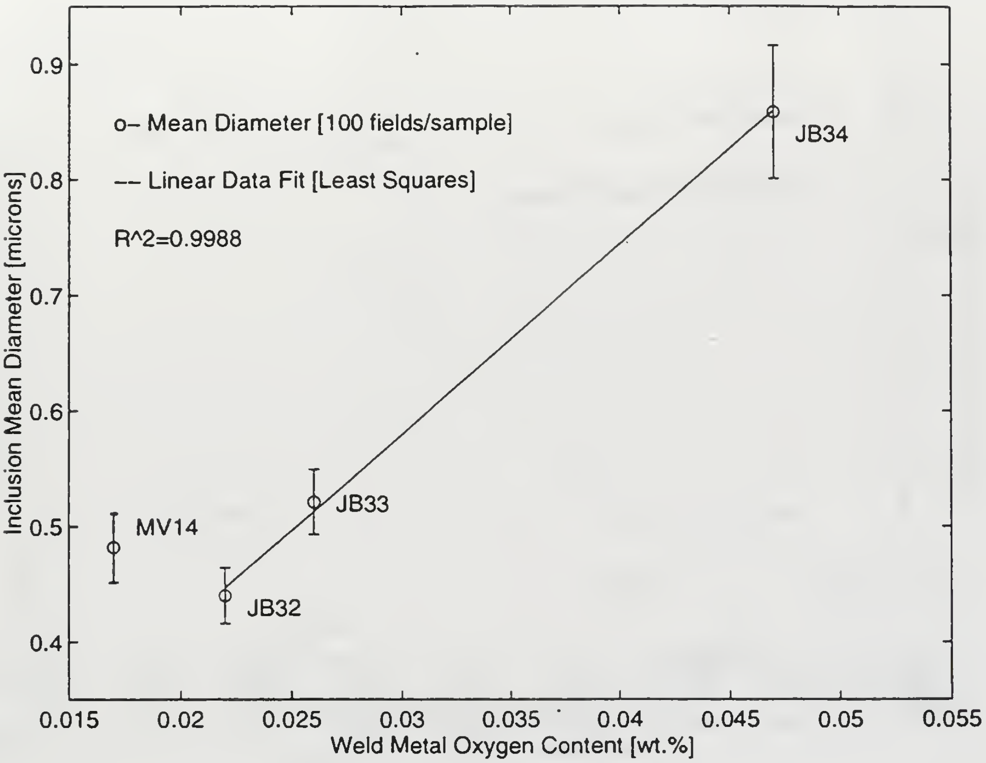

| Sample I. D. | Oxygen Content [wt. %] | Mean Diameter [microns] |
|---|---|---|
| MV14 | 0.017 | 0.4818 |
| JB32 | 0.022 | 0.4397 |
| JB33 | 0.026 | 0.5208 |
| JB34 | 0.047 | 0.8575 |

Figure 4-4 Inclusion Mean Diameter vs. Weld Metal Oxygen Content

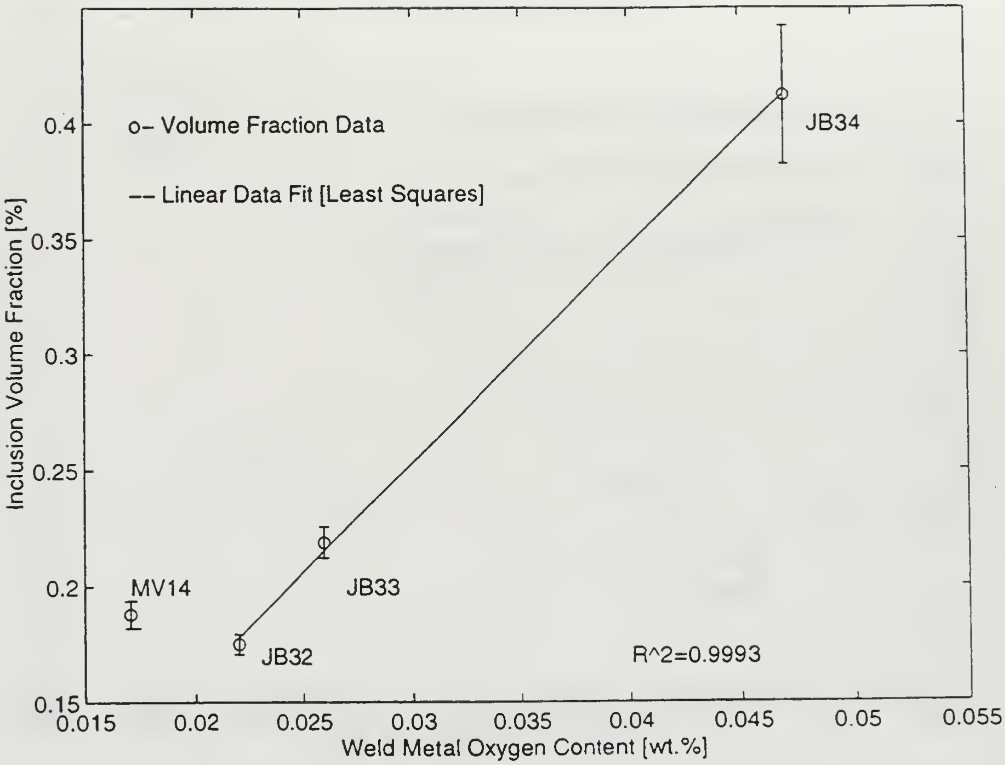

| Sample I.D. | Oxygen Content [wt. %] | Volume fraction [%] |
|---|---|---|
| MV14-9 | 0.017 | 0.188 |
| JB32 | 0.022 | 0.175 |
| JB33 | 0.026 | 0.219 |
| JB34 | 0.047 | 0.412 |

Figure 4-5 Inclusion Volume Fraction vs. Weld Metal Oxygen Content

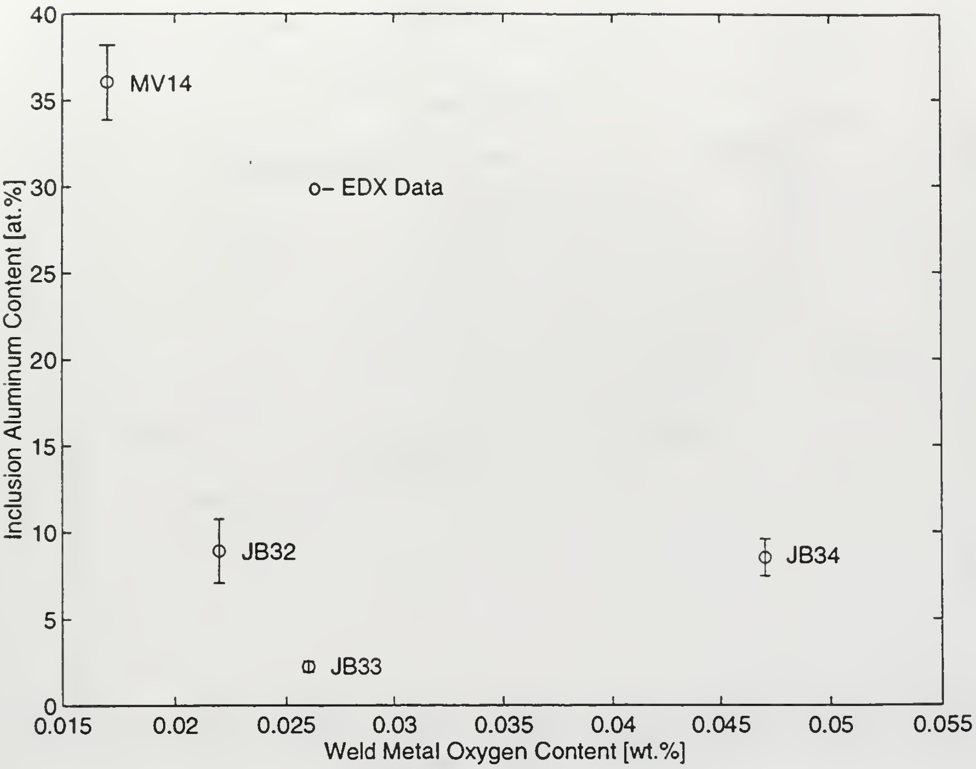

| Sample I.D. | Weld Metal Oxygen Content[wt%] | Inclusion Aluminum Content [at%] |
|---|---|---|
| MV14 | 0.017 | 36.06 |
| JB32 | 0.022 | 8.93 |
| JB33 | 0.026 | 2.24 |
| JB34 | 0.047 | 8.53 |

Figure 4-6 Inclusion Aluminum Content vs. Weld Metal Oxygen Content

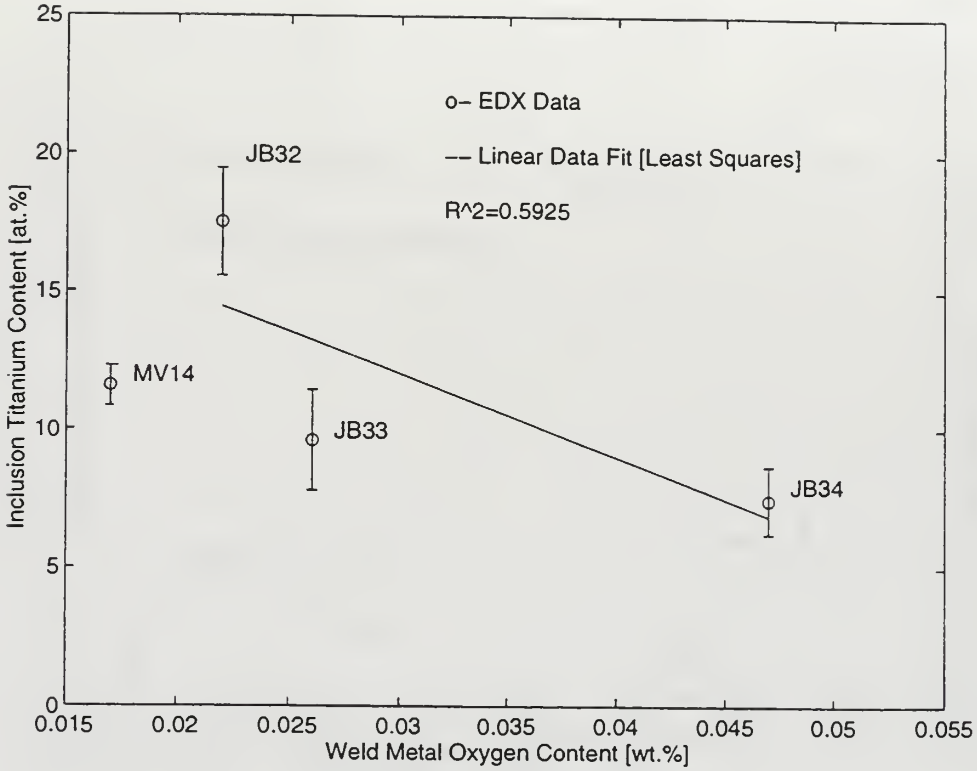

| Sample I.D. | Weld Metal Oxygen Content[wt%] | Inclusion Titanium Content [at%] |
|---|---|---|
| MV14 | 0.017 | 11.60 |
| JB32 | 0.022 | 17.52 |
| JB33 | 0.026 | 9.62 |
| JB34 | 0.047 | 7.46 |

Figure 4-7 Inclusion Titanium Content vs. Weld Metal Oxygen Content

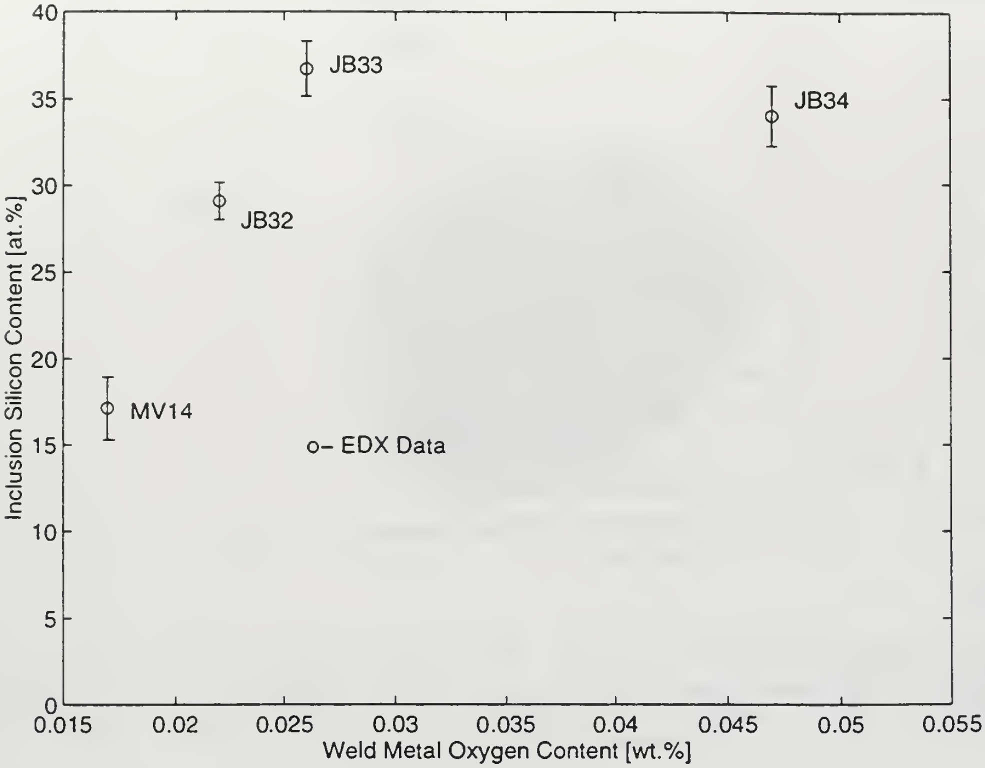

| Sample I.D. | Weld Metal Oxygen Content[wt%] | Inclusion Silicon Content [at%] |
|---|---|---|
| MV14 | 0.017 | 17.14 |
| JB32 | 0.022 | 29.07 |
| JB33 | 0.026 | 36.71 |
| JB34 | 0.047 | 34.00 |

Figure 4-8 Inclusion Silicon Content vs. Weld Metal Oxygen Content

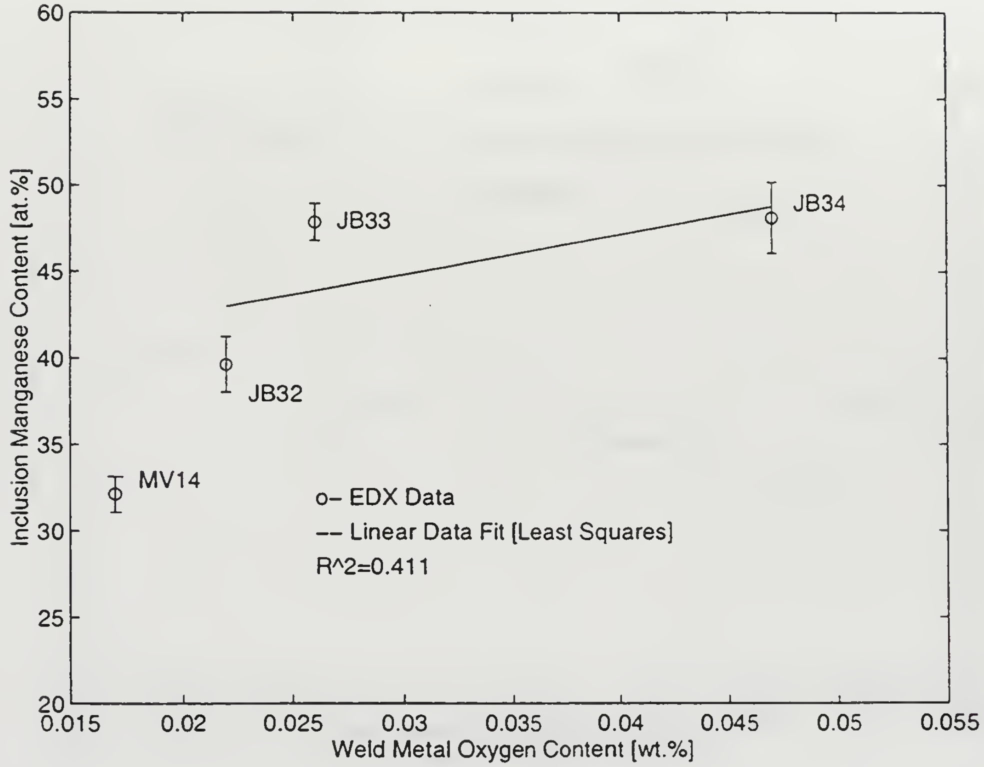

| Sample I.D. | Weld Metal Oxygen Content[wt%] | Inclusion Manganese Content [at%] |
|---|---|---|
| MV14 | 0.017 | 32.15 |
| JB32 | 0.022 | 39.64 |
| JB33 | 0.026 | 47.88 |
| JB34 | 0.047 | 48.10 |

Figure 4-9 Inclusion Manganese Content vs. Weld Metal Oxygen Content

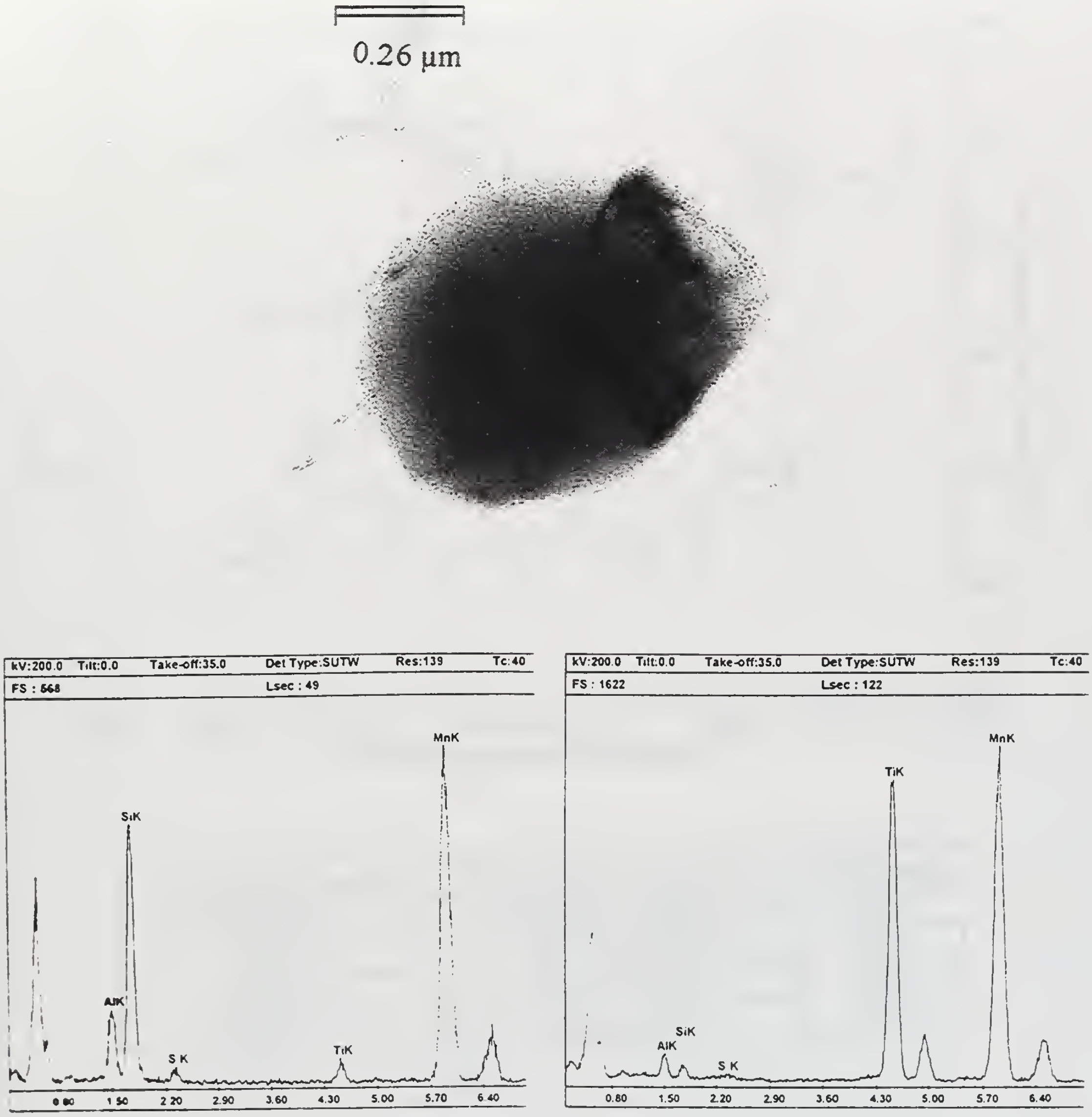

(a)

(b)

Figure 4-10 TEM photo of Multi-phase Inclusion and EDX Spectra From (a) Light Region, (b) Dark and Faceted Region

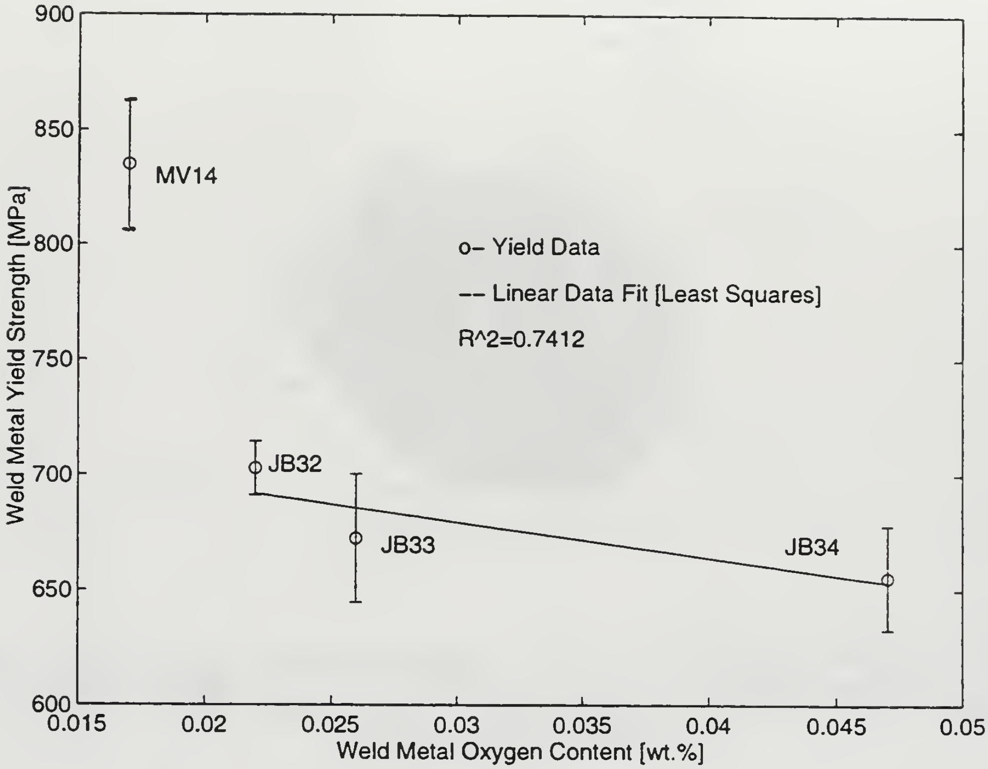

| Sample ID | Yield Strength [Mpa] (ksi) | Oxygen Content [wt.%] |
|---|---|---|
| MV14 | 834.91 (121.19) | 0.017 |
| JB32 | 702.86 (102.20) | 0.022 |
| JB33 | 672.53 (97.62) | 0.026 |
| JB34 | 655.43 (95.14) | 0.047 |

Figure 4-11 Weld Metal Yield Strength vs. Weld Metal Oxygen Content

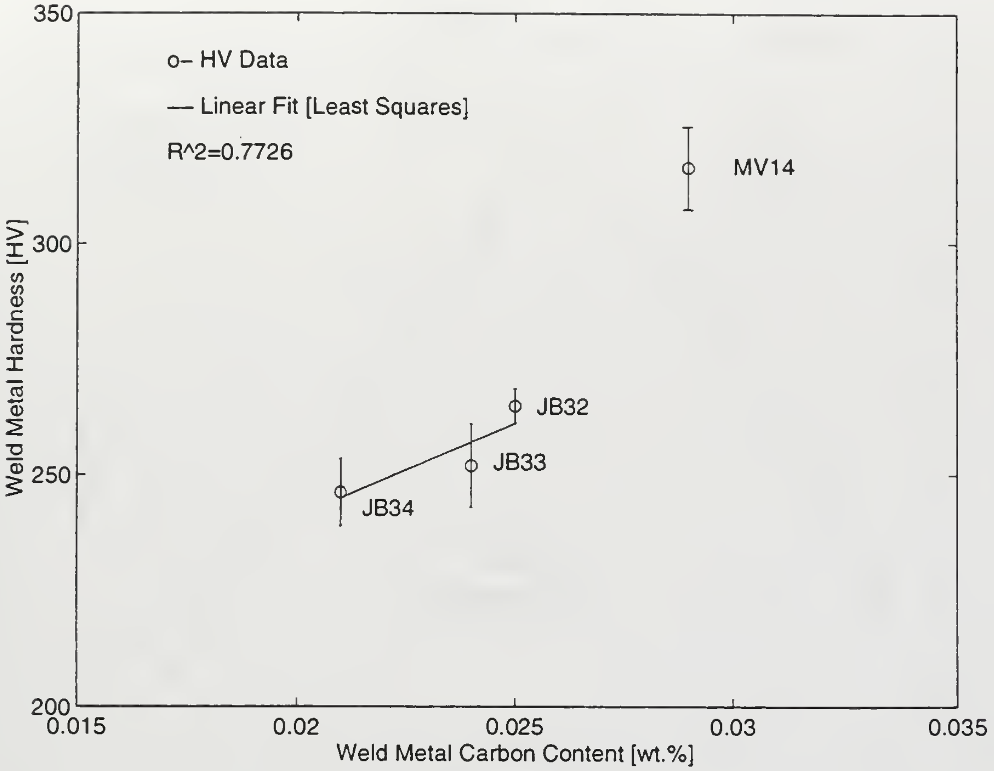

| Sample I.D. | Hardness [Vickers] | Carbon Content [wt.%] |
|---|---|---|
| MV14 | 316.54 | 0.029 |
| JB32 | 264.92 | 0.025 |
| JB33 | 252.05 | 0.024 |
| JB34 | 246.27 | 0.021 |

Figure 4-12 Weld Metal Hardness vs. Weld Metal Carbon Content

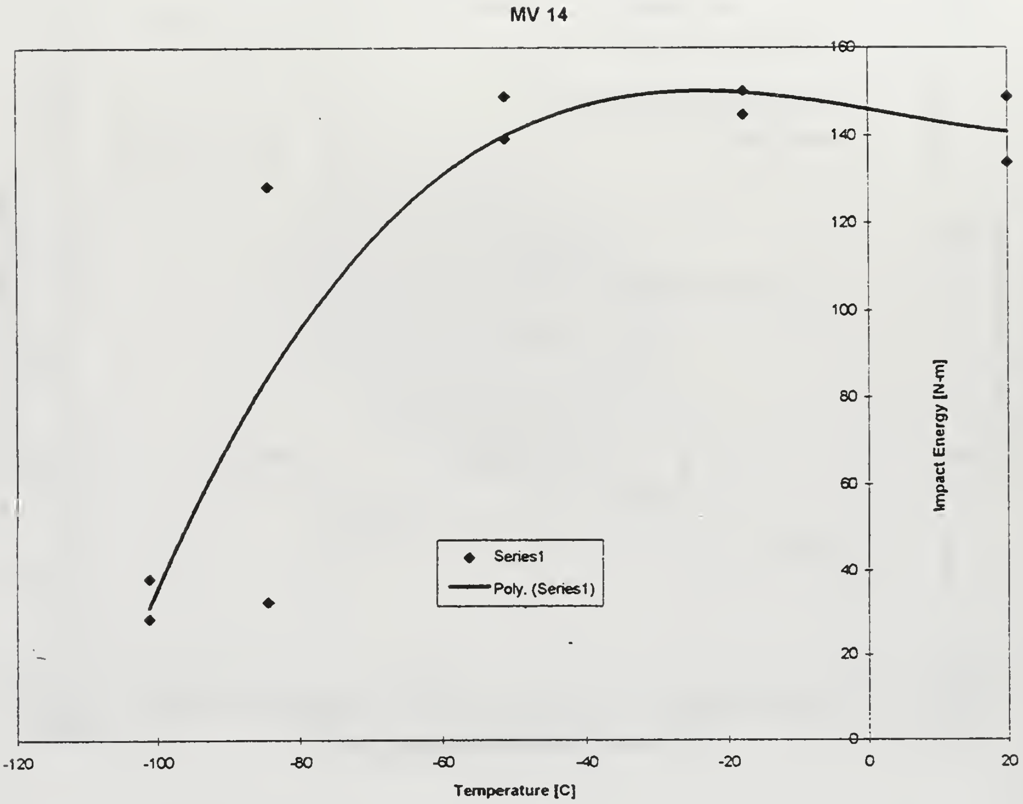

| Sample I.D. | Hardness [Vickers] | FATT [deg C] | Carbon Content [wt.%] |
|---|---|---|---|
| MV14 | 316.54 | -89.44 | 0.029 |
| JB32 | 264.92 | -70.56 | 0.025 |
| JB33 | 252.05 | -42.78 | 0.024 |
| JB34 | 246.27 | -42.78 | 0.021 |

Figure 4-13 MV14 Charpy Impact Data (Data Provided by NSWC)

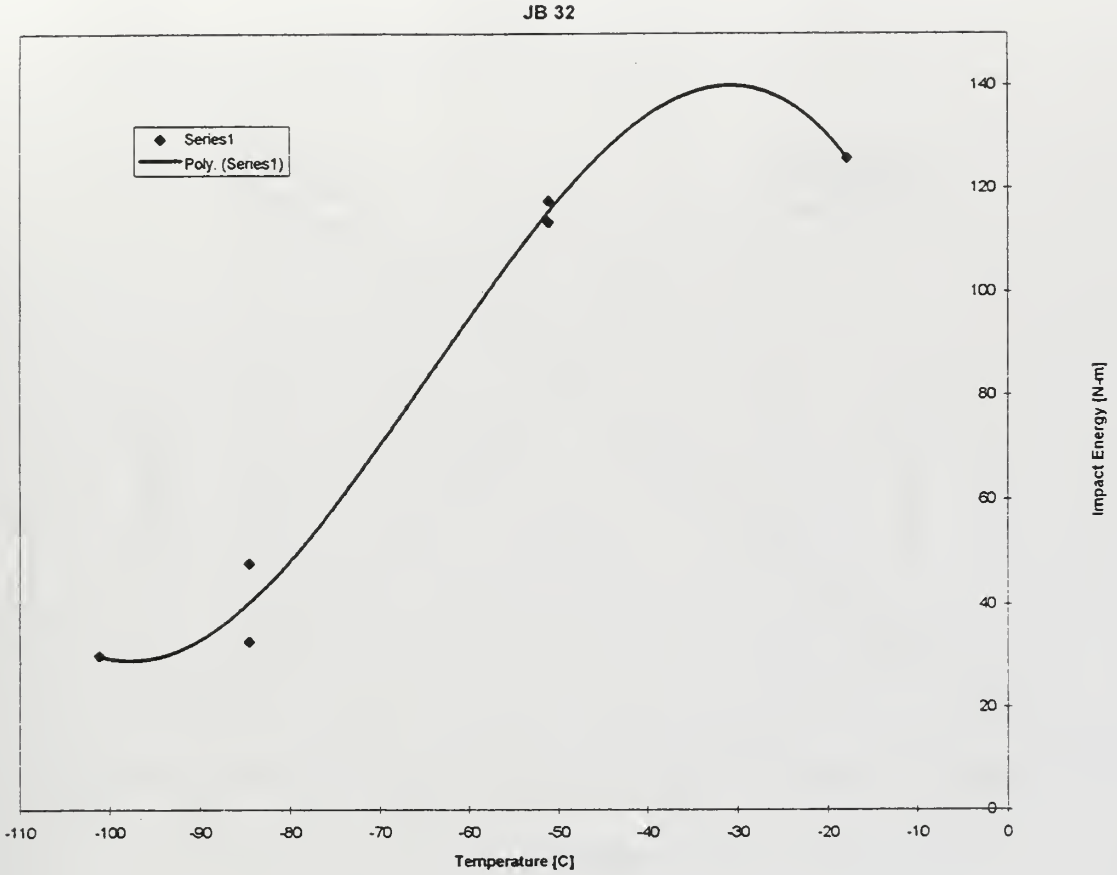

| Sample I.D. | Hardness [Vickers] | FATT [deg C] | Carbon Content [wt.%] |
|---|---|---|---|
| MV14 | 316.54 | -89.44 | 0.029 |
| JB32 | 264.92 | -70.56 | 0.025 |
| JB33 | 252.05 | -42.78 | 0.024 |
| JB34 | 246.27 | -42.78 | 0.021 |

Figure 4-14 JB32 Charpy Impact Data (Data Provided by NSWC)

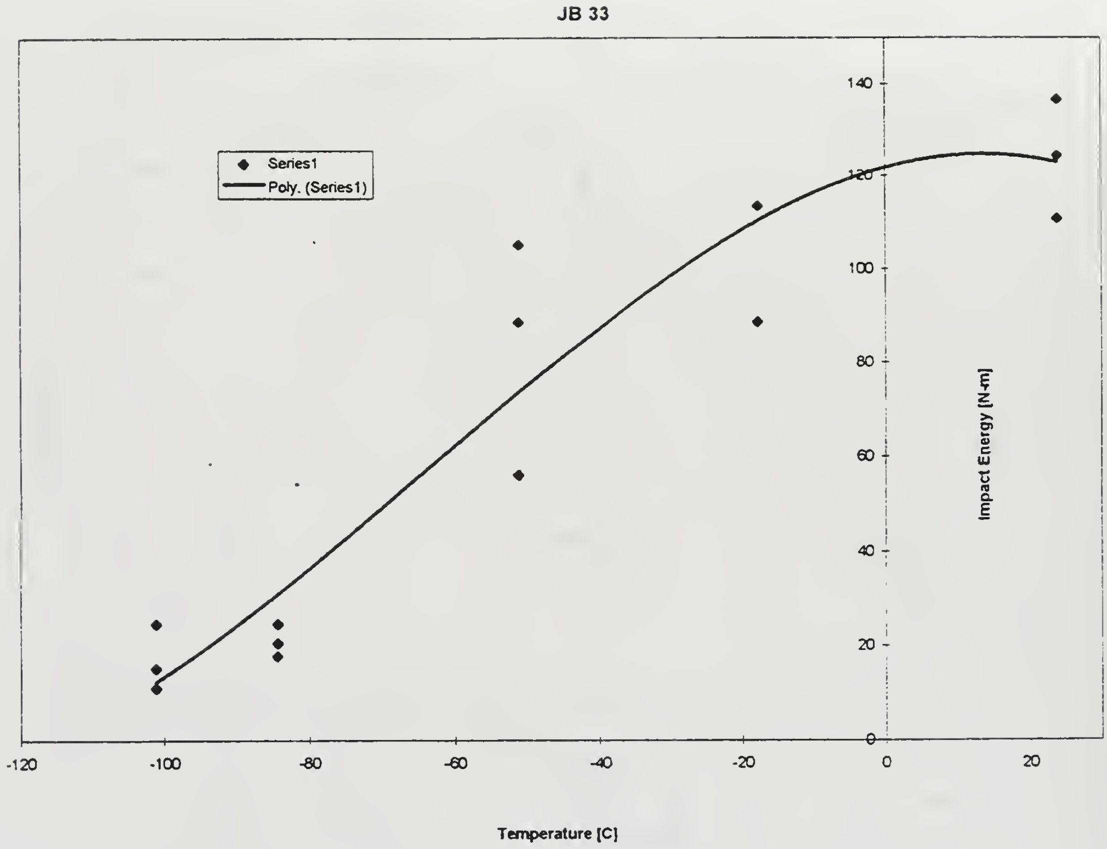

| Sample I.D. | Hardness [Vickers] | FATT [deg C] | Carbon Content [wt.%] |
|---|---|---|---|
| MV14 | 316.54 | -89.44 | 0.029 |
| JB32 | 264.92 | -70.56 | 0.025 |
| JB33 | 252.05 | -42.78 | 0.024 |
| JB34 | 246.27 | -42.78 | 0.021 |

Figure 4-15 JB33 Charpy Impact Data (Data Provided by NSWC)

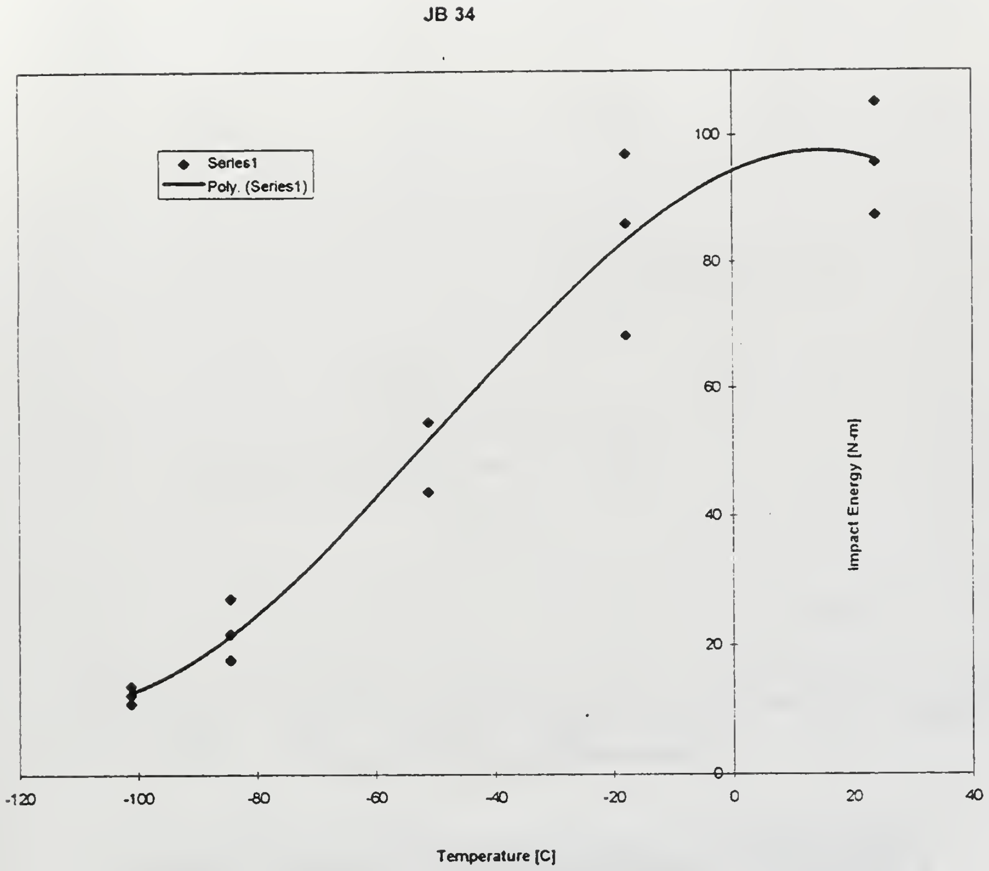

| Sample I.D. | Hardness [Vickers] | FATT [deg C] | Carbon Content [wt.%] |
|---|---|---|---|
| MV14 | 316.54 | -89.44 | 0.029 |
| JB32 | 264.92 | -70.56 | 0.025 |
| JB33 | 252.05 | -42.78 | 0.024 |
| JB34 | 246.27 | -42.78 | 0.021 |

Figure 4-16 JB34 Charpy Impact Data (Data Provided by NSWC)

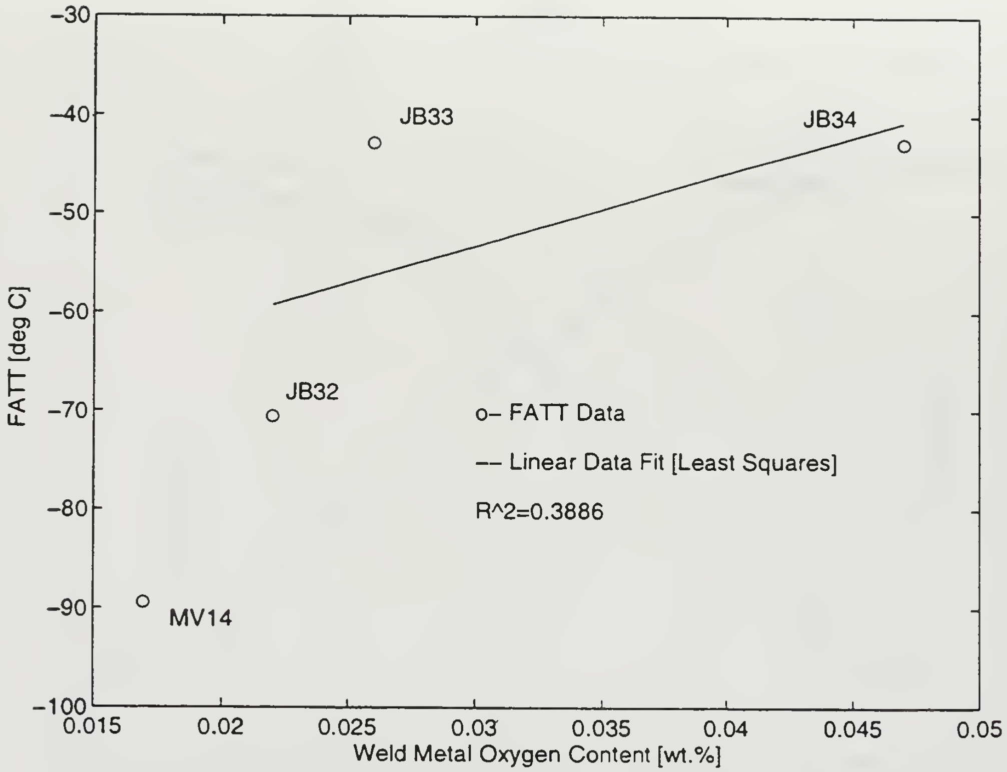

| Sample ID | Oxygen Content [wt.%] | FATT [deg C] (deg F) |
|---|---|---|
| MV14 | 0.017 | -89.44 (-129.0) |
| JB32 | 0.022 | -70.56 (-95.0) |
| JB33 | 0.026 | -42.78 (-45.0) |
| JB34 | 0.047 | -42.78 (-45.0) |

Figure 4-17 Fracture Appearance Transition Temperature vs. Weld Metal Oxygen Content

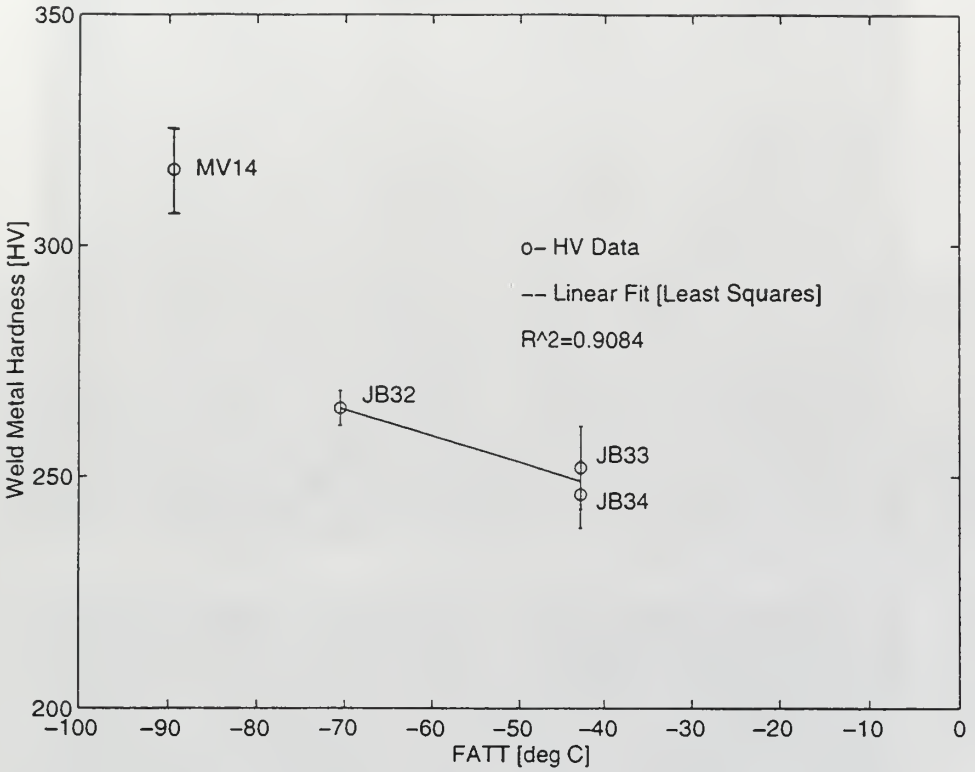

| Sample I.D. | Hardness [Vickers] | FATT [deg C] | Carbon Content [wt.%] |
|---|---|---|---|
| MV14 | 316.54 | -89.44 | 0.029 |
| JB32 | 264.92 | -70.56 | 0.025 |
| JB33 | 252.05 | -42.78 | 0.024 |
| JB34 | 246.27 | -42.78 | 0.021 |

Figure 4-18 Weld Metal Hardness vs. Fracture Appearance Transition Temperature

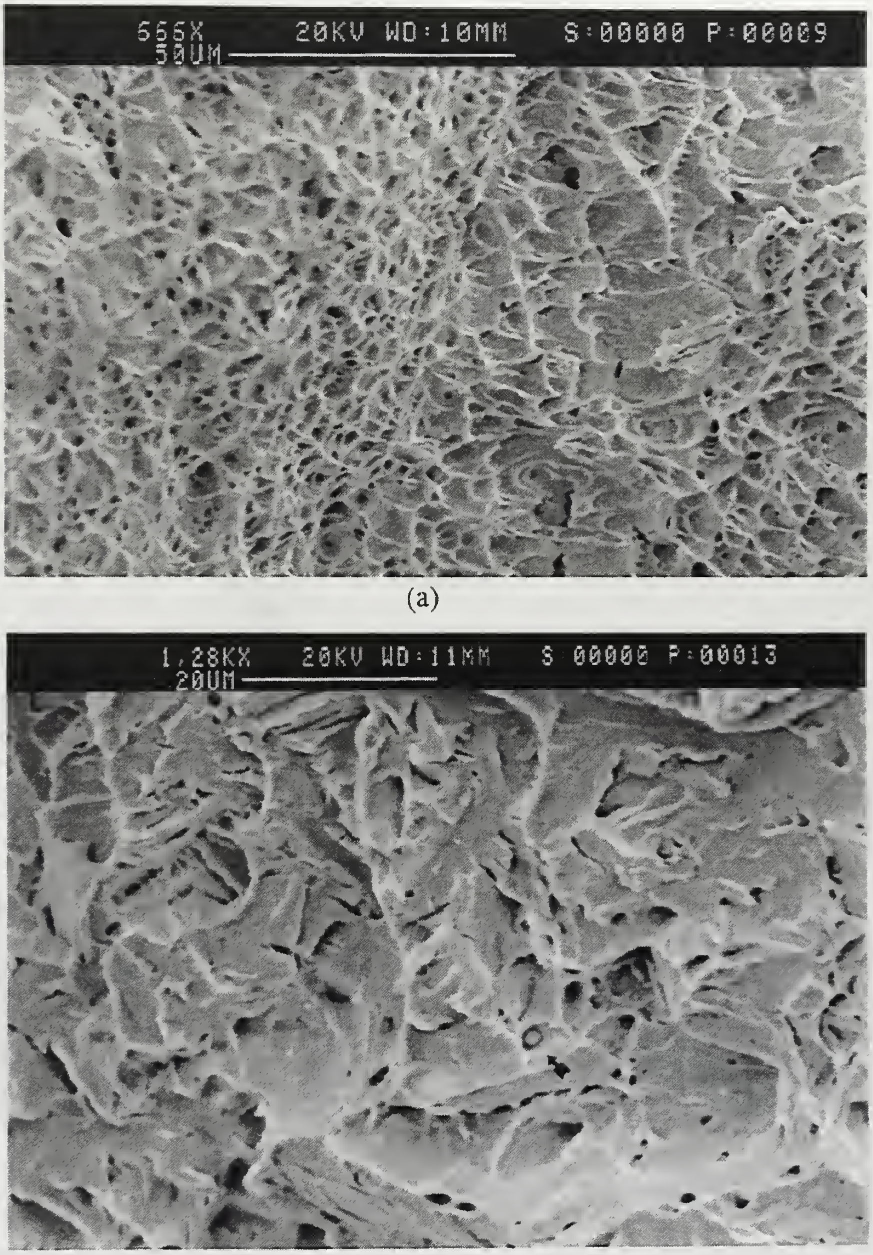
566X 20KV WD:10MM S:00000 P:00009
50UM
1.28KX 20KV WD:11MM S:00000 P:00013
20UM

(a)

(b)

Figure 4-19 SEM Micrographs of MV14 (a) Upper , and (b) Lower , Charpy V-notch Fracture Surfaces

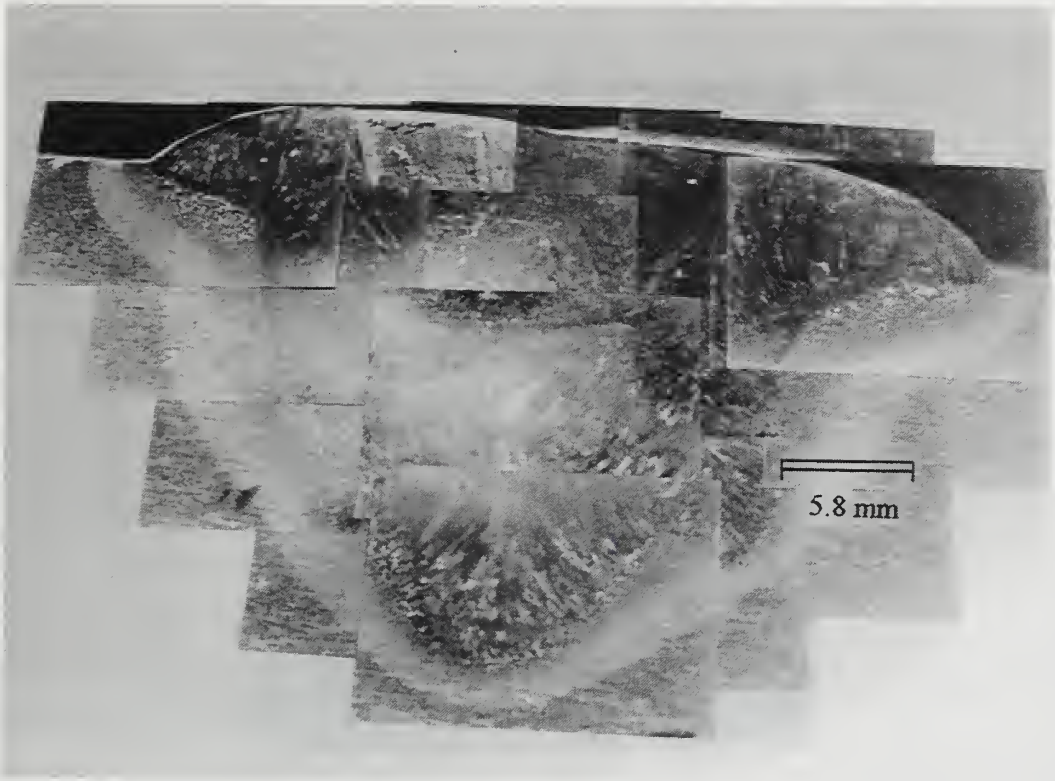

Figure 4-20 Representative Macrograph of a Gas Metal Arc Weld

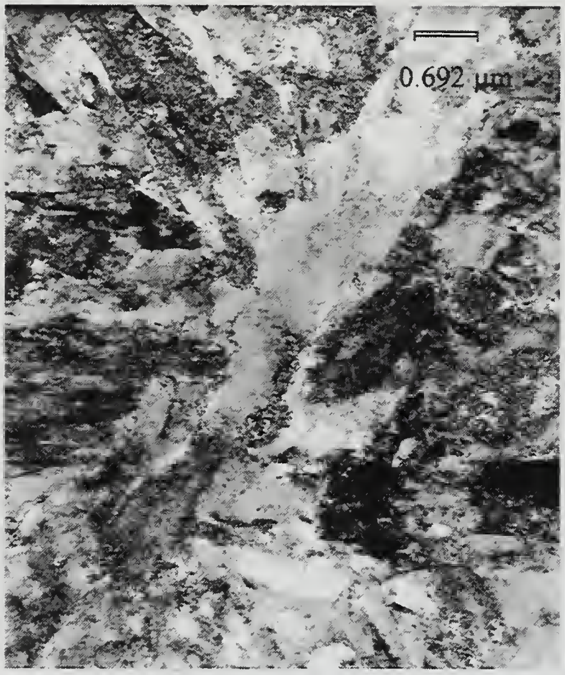

Figure 4-21 TEM Bright Field Micrograph of Representative Weld Metal Microstructure

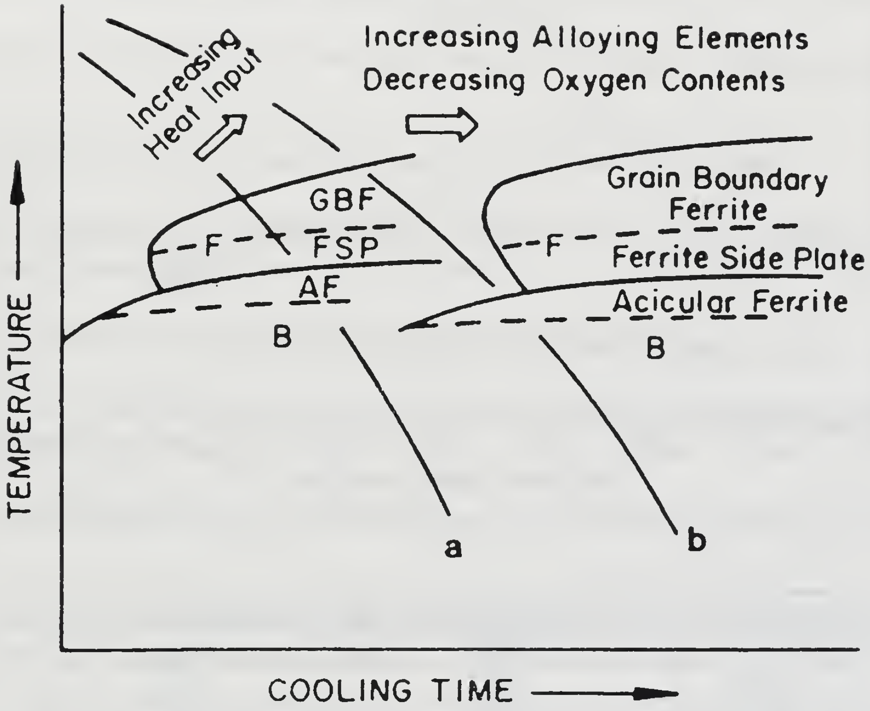
Increasing Heat Input
Increasing Alloying Elements
Decreasing Oxygen Contents
GBF
F
FSP
AF
B
Grain Boundary Ferrite
F
Ferrite Side Plate
Acicular Ferrite
B
a
b
TEMPERATURE
COOLING TIME

Figure 4-22 Representative Weld Metal Continuous Cooling Transformation Diagram [from Ref.4]

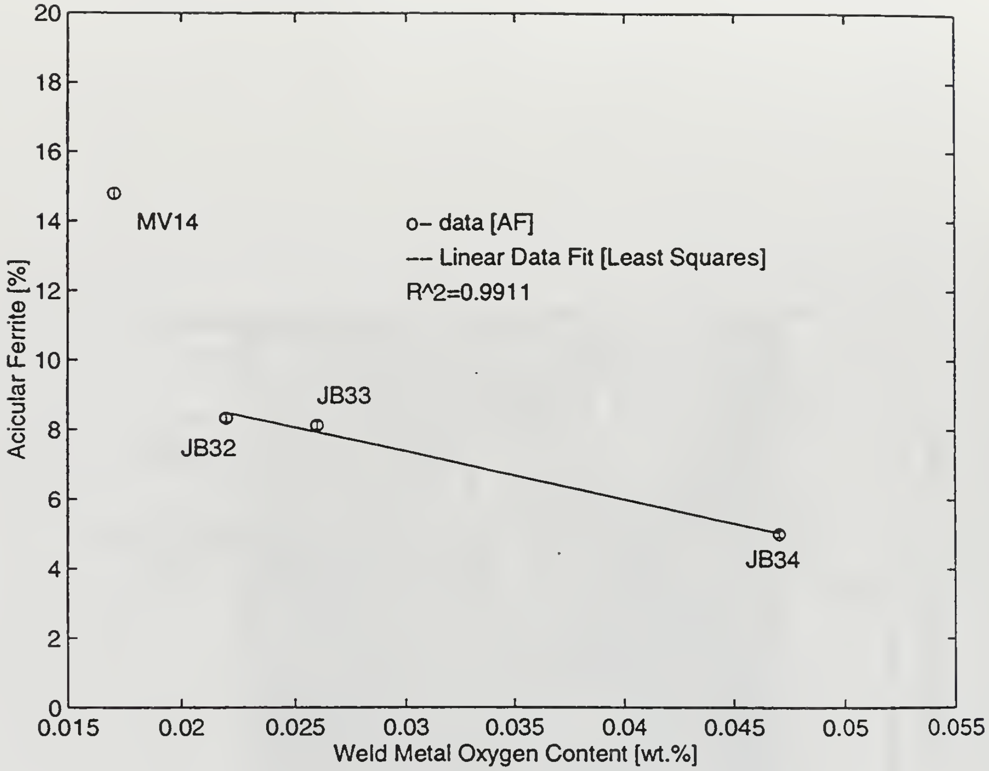

| Sample I.D. | Weld Metal Oxygen Content [wt%] | Acicular Ferrite [%] |
|---|---|---|
| MV14 | 0.017 | 14.8 |
| JB32 | 0.022 | 8.3 |
| JB33 | 0.026 | 8.1 |
| JB34 | 0.047 | 5.0 |

Figure 4-23 Acicular Ferrite vs. Weld Metal Oxygen Content

# LIST OF REFERENCES

1. Deloach, Jr.,J.J., Franke, G.L., Vassilaros, M.G., Wong,R.J. and Denale,R., "Current Welding Consumables Research in the U.S. Navy," Carderock Division, Naval Surface Warfare Center CARDIVNSWC-SSM-61-93/09, March, 1993 .

2. Department of the Navy Military Specification MIL-E-23765/2E(SH), *Electrodes and Rods-Welding, Bare, Solid, or Alloy Cored; and Fluxes, Low Alloy Steel,* 22 April 1994.

3. Callister W.D., *Materials Science and Engineering: an Introduction*, John Wiley and Sons, *1991.*

4. Kou, S,. *Welding Metallurgy,* John Wiley and Sons, Inc., New York, 1987.

5. Grong, O., Matlock, D.K., "Microstructural Development in Mild and Low-Alloy Steel Weld Metals"*, International Metals reviews,* v. 31, 1986

6. Brumbaugh, James E., *Welders Guide,* Macmillan Publishing Company, 1986.

7. Widgery, A.D., "Deoxidation Practice for Mild Steel Weld Metal," *Welding Research Supplement,* March, 1976.

8. Liu, S., "Metallography of HSLA Steel Weldments," *Key Engineering Materials,* Vol. 69-70 1992.

9. Liu, S., Olsen, D.L., "The Role of Inclusions in Controlling HSLA Steel Weld Microstructure", *Welding Research Supplement,* June 1986.

10. Dowling, J.M., Corbett, J.M., Kerr, H.W., "Inclusion Phases and the Nucleation of Acicular Ferrite in Submerged Arc Welds in High Strength Low Alloy Steels", *Metallurgical Transactions A,* 1986.

11. Harrison, P.L., Farrar, R.A., "Application of Continuous Cooling Transformation Diagrams for Welding of Steels", *International Materials Reviews,* Vol. 34, No. 1, 1989.

12. Fox, A.G., Brothers, D.G., "The Role of Titanium in the non-Metallic Inclusions Which Nucleate Acicular Ferrite in the Submerged Arc Weld (SAW) Fusion Zones of Navy HY-100 Steel", *Scripta Metallurgica et Materiala,* 1995.

13. Babu, S.S., David, S.A., Vitek, J.M., Mundra, K., Debroy, T., 'Development of Macro- and Microstructures of Carbon-Manganese Low Alloy Steel Welds: Inclusion Formation", *Materials Science and Technology,* 1995.

14. Ricks, R.A., Howell, P.R., Barrite, G.S., "The Nature of Acicular Ferrite in HSLA Steel Weld Metals", *Journal of Material Science,* 1982.

15. Thompson, S.W., Colvin, D.J., Krauss, G.," Continuous Cooling Transformations and Microstructures in a Low-Carbon, High-Strength Low-Alloy Plate Steel", *Metallurgical Transactions A,* Vol. 21A, June 1990.

16. Fox, A.G., Eakes, M.W., Wong, R., "The Effect of Gas Composition on the Microstructure and Mechanical Properties of Gas-Metal-Arc-Weld Metal of Navy HSLA-100 Steels", submitted, *Welding Research Supplement to The Welding Journal,* 1995.

17. Fox, A.G., Blackburn, J.M., Vassilaros, M., " Factors Affecting the Impact Toughness of Low Carbon Bainitic Weld Metal", Paper Presented Fourth International Conference of Trends in Welding Research, Gatlinburg, Tennessee, June 1995

18. Pickering, F.B., *Physical Metallurgy and the Design of Steels,* Applied Science Publishers Ltd., London, 1978.

19. Reck, V., Jr., *Mechanical and Microstructural Properties of Ultra-Low Carbon Bainitic Steel Weld Metal,* Masters Thesis, Naval Postgraduate School, Monterey, CA., 1995.

20. Smallman, R.E., *Modern Physical Metallurgy*, Butterworth-Heinemann Ltd., Oxford, 1992.

21. DeHoff, R.T., Rhines, F.N., *Quantitative Microscopy,* McGraw-Hill Inc., 1968

22. Clark, A.L., *The Effect of Varying the MnO Content of the Flux Used for the Submerged Arc Welding of Navy HY-100 Steel,* Masters Thesis, Naval Postgraduate School, Monterey, CA., 1995.

23. ASTM Standard E 562-89, "Standard Test Method for Determining Volume Fraction by Systematic Manual Point Count", *Annual Book of ASTM Standards,* 1995.

24. Gladman, T., Woodhead, J.H., "The Accuracy of Point Counting in Metallographic Investigations", *Journal of the Iron and Steel Institute,* February, 1960.

25. Mischke, C.R., Shigley, J.E., *Mechanical Engineering Design,* McGraw-Hill, Inc., 1989

26. Beckwith, T.G., Lienhard V, J.H., Marangoni, R.D., *Mechanical Measurements,* Addison-Wesley Publishing Company, Fifth Edition, 1995.

27. Fox, A.G., Eakes, M.W., Franke, G.L., " The Effect of Small Changes in Flux Basicity on the Acicular Ferrite Content and Mechanical Properties of Submerged Arc Weld Metal of Navy HY-100 Steel", accepted for publication in *Welding Research Supplement to the Welding Journal.*

28. Onsoien, M.I., Liu, S., Olson, D.L., "Shielding Gas Oxygen Equivalent in Weld Metal Microstructure Optimization", *Welding Research Supplement to the Welding Journal,* July, 1996.

## INITIAL DISTRIBUTION LIST

No. Copies

1. Defense Technical Information Center
   8725 John J. Kingman Road, Ste 0944
   Ft. Belvoir, Virginia 22060-6218 ....................2

2. Dudley Knox Library
   Naval Postgraduate School
   411 Dyer Rd.
   Monterey, California 93943-5101 ....................2

3. Naval/Mechanical Engineering Curricular Offce, Code 34
   Naval Postgraduate School
   Monterey, California 93943-5000 ....................1

4. Department Chairman, Code ME
   Department of Mechanical Engineering
   Naval Postgraduate School
   Monterey, California 93943-5000 ....................1

5. Dr. Alan G. Fox, Code ME/FX
   Department of Mechanical Engineering
   Naval Postgraduate School
   Monterey, California 93943-5000 ....................2

6. Mr. Joe Blackburne
   Naval Surface Warfare Center
   Carderock Division, Code 615
   9500 McArthur Boulevard
   Bethesda, Maryland 20084-5000....................1

7. Mr. R. DeNale
   Naval Surface Warfare Center
   Carderock Division, Code 615
   9500 McArthur Boulevard
   Bethesda, Maryland 20084-5000....................1

8. Mary E. Gwin
   105 Magnolia Street
   Trussville, Alabama 35173 ....................2

DUDLEY KNOX LIBRARY
NAVAL POSTGRADUATE SCHOOL
MONTEREY CA 93943-5101

DUDLEY KNOX LIBRARY
3 2768 00324276 9